DOKUZ EYLÜL UNIVERSITY
GRADUATE SCHOOL OF NATURAL AND APPLIED SCIENCES

INVESTIGATION OF FLOW CHARACTERISTICS OF HOUSEHOLD APPLIANCES BY PARTICLE IMAGE VELOCIMETRY

by

Gürkan ÇALIŞKAN

July, 2016

İZMİR

INVESTIGATION OF FLOW CHARACTERISTICS OF HOUSEHOLD APPLIANCES BY PARTICLE IMAGE VELOCIMETRY

A Thesis Submitted to the
Graduate School of Natural and Applied Sciences of Dokuz Eylül University
In Partial Fulfillment of the Requirements for the Degree of Master of Science
in Mechanical Engineering, Energy Program

by

Gürkan ÇALIŞKAN

July, 2016

İZMİR

M.Sc THESIS EXAMINATION RESULT FORM

We have read the thesis entitled **"INVESTIGATION OF FLOW CHARACTERISTICS OF HOUSEHOLD APPLIANCES BY PARTICLE IMAGE VELOCIMETRY"** completed by **GÜRKAN ÇALIŞKAN** under supervision of **PROF. DR. DİLEK KUMLUTAŞ** and we certify that in our opinion it is fully adequate, in scope and in quality, as a thesis for the degree of Master of Science.

Prof. Dr. Dilek KUMLUTAŞ

Supervisor

Prof. Dr. İsmail Hakkı Tavman

(Jury Member)

A. Özdamar

Prof. Dr. Aydoğan Özdamar

(Jury Member)

Prof.Dr. Ayşe OKUR
Director
Graduate School of Natural and Applied Sciences

ACKNOWLEDGEMENTS

First of all, I would like to express deepest gratitude to my supervisor Prof. Dr. Dilek KUMLUTAŞ for her full support, expert guidance, understanding and encouragement throughout my study and research. Without her incredible patience, timely wisdom and counsel, moral support and valuable advices, my thesis work would have been a frustrating and overhelming pursuit.

I also wish to express my gratitude to Project Assistant Özgün ÖZER for his motivation, support and sharing their valuable experiences with me.

Also, I would like to express special thanks to my friends for their motivation and help.

Finally, I would like to thank to my family for their invaluable support, encouragement and patience throughout my entire life.

Gürkan ÇALIŞKAN

INVESTIGATION OF FLOW CHARACTERISTICS OF HOUSEHOLD APPLIANCES BY PARTICLE IMAGE VELOCIMETRY

ABSTRACT

The aim of this study is to investigate geometrical design parameters effects of an outdoor unit of a split type air conditioner on axial fan performance. When the literature has been investigated, it has seen that there is no study which is about investigating flow structure of an outdoor unit of a split type air conditioner by implementing numerical methods. Within this study, an outdoor unit of a split type air conditioner was modelled three dimensionally and solved under transient state condition by using Computational Fluid Dynamics (CFD) method. On the other hand, Particle Image Velocimetry (PIV) was used to investigate velocity distribution and average velocity value on outdoor unit's exit plane. This experimental method was also used for validating numerical model. In addition, CFD results were verified by another experimental method which measures average mass flow rate of air passing through outdoor unit's exit plane.

After verifying the numerical model, parametric study was performed. The pressure and flow coefficients, which are mostly used to express fan performance in literature, were calculated by using the results which were obtained from parametric analyses. The computational results showed that nozzle depth and diameter, fan position and heat exchanger position play important roles in changing performance coefficients.

Keywords: Split type air conditioner, outdoor unit, computational fluid dynamics, particle image velocimetry

BEYAZ EŞYALARDA AKIŞ KARAKTERİSTİKLERİNİN PARÇACIK GÖRÜNTÜLEMELİ HIZ ÖLÇÜMÜ YÖNTEMİ İLE İNCELENMESİ

ÖZ

Bu çalışmanın amacı, bir split klima dış ünitesine ait geometrik tasarım parametrelerinin eksenel fan performansına etkilerinin incelenmesidir. Literatür araştırması sonucunda, sayısal yöntemleri kullanarak bir split klima dış ünitesinin akış yapısının incelendiği bir çalışmanın olmadığı görülmüştür. Bu çalışma kapsamında, bir split klima dış ünitesi üç boyutlu olarak modellenmiş ve Hesaplamalı Akışkanlar Dinamiği (HAD) yöntemiyle zamana bağlı olarak çözülmüştür. Diğer taraftan, dış ünitenin çıkış düzlemindeki hız dağılımı ve hız değerlerini incelemek için Parçacık Görüntülemeli Hız Ölçümü (PGHÖ) yöntemi kullanılmıştır. Bu deneysel yöntem aynı zamanda sayısal modeli doğrulamak için de kullanılmıştır. Ek olarak, HAD sonuçları, bir başka deneysel yöntem yardımıyla, dış ünitenin çıkış düzleminden geçen hava debisinin ölçülmesiyle de doğrulanmıştır.

Sayısal model doğrulandıktan sonra, parametrik çalışma yapılmıştır. Parametrik analizlerden elde edilen sonuçlar kullanılarak, literatürde fan performansını ifade etmede sıklıkla kullanılan basınç ve akış katsayıları hesaplanmıştır. Sayısal sonuçlar, nozul çap ve derinliği, fan pozisyonu ve ısı eşanjörü poziyonunun performans katsayılarını değiştirmede önemli rol oynadığını göstermiştir.

Anahtar kelimeler: Split klima, dış ünite, hesaplamalı akışkanlar dinamiği, parçacık görüntülemeli hız ölçümü

CONTENTS

LIST OF FIGURES

LIST OF TABLES

CHAPTER ONE
INTRODUCTION TO SPLIT AIR CONDITIONERS

1.1 Literature Survey

Air conditioning is the process of altering the properties of air to more comfortable conditions, typically with the aim of distributing the conditioned air to an occupied space such as a building, house or vehicle to improve thermal comfort and indoor air quality.

Split types of air conditioners have a wide use at the present time. These conditioners consist of two units, one is indoor unit and the other one is outdoor unit. In this chapter, the studies which are about outdoor unit of a split air conditioner in literature have been told mostly.

In 2000, Chow, Lin and Wang have studied over split-type air-conditioners in high-rise residential buildings which became trendy in Hong Kong. They had some investigations on different re-entrant shapes by using computational fluid dynamics techniques together with an energy evaluation model. The results showed that the new re-entrant shapes wouldn't have adverse effects when comparing with the conventional design.

Another similar study is the paper which was written by Chow, Lin and Liu (2002). Based on computational fluid dynamics analysis incorporating with energy evaluation model, they have searched the effectiveness of different condenser order schemes in building re-entrants by taking account of steady state conditions. It was found that there were limited hard-and-fast rules to give definite solutions. Provided that there was no physical access problem, an alignment of condensing units facing inward to induce a positive inflow air into the re-entrant was a desirable solution.

Hu and Huang (2005) have studied experimentally on cooling air in outdoor unit of a split air conditioner by water. A cooling tower was integrated with outdoor unit.

The cooling tower consisted of a water sprayer and a cellulose pad which had good water wettability and caused a uniform water film over the entire surface of the pads and a perfect contact between water and cooling air. Their experimental results showed that the coefficient of performance (COP) reached 3.45 and that was higher than the standard value (2.96) of those conventional residential split air conditioners.

In order to analyse the influence of the deflecting ring on the noise generated by the outdoor unit of a split type air conditioner, Hu and Ding (2006) simulated the flow field in the outdoor set with the CFD software STAR-CD. After they investigated numerically, they validated experimentally their numerical results. The results of computation and experiment showed that there was an optimal width of the deflecting ring, corresponding to the minimum noise generated by the outdoor unit. In addition, they designed a double contoured duct and analysed it, too. The results of computation and experiment verify that the deflecting ring with double contoured duct could increase the aerodynamic performance and decrease the noise generated by the outdoor unit.

Hu and Ding (2006) have investigated the influence of the air outlet louver on the noise generated by the outdoor unit of a split type air conditioner in their another study. They analysed the influence of the shape and the steel wire diameter of the air outlet louver on the noise generated by the outdoor unit. The results of computation and experiment showed that the circular shape of air outlet louver reduced noise level. An air outlet louver with various diameters of steel wires was designed on the basis of analysis of the influence of the steel wire diameter of the air outlet louver on the noise. The computation and experiment validated that the air outlet louver with various diameters of steel wires could increase the aerodynamic performance and decrease the noise generated by the outdoor unit.

In another study, optimum placement has been investigated for outdoor unit of a split type air conditioner. Avara and Daneshgar (2008) have searched about installation distance from the supporting wall and the height of installation by using CFD. These were two factors that affect the outdoor unit efficiency. Analyses have been done for outdoor unit between two walls and outdoor unit on the roof. In the result of investigating, optimum installation distance and height have been determined.

A paper about outdoor unit noise reduction by modifying fan design has been published by Zhao, Sun and Zhang (2013). Computational fluid dynamics and computational aerodynamic acoustics have been utilized to estimate the noise behaviour. The aeroacoustic test was done in an anechoic chamber. The results were compared with the semi-anechoic chamber ones, and the unremarkable differences were produced, which indicated the ground floor being of some influence. The results showed that both modified fan designs were effective to decrease the noise but the flanging outer-edge blade was more efficient. The noise directivities of three different fan designs were investigated both numerically and experimentally and the produced asymmetric characteristics were analysed.

Another paper of Zhao, Sun, Wang and Zhang (2014) is about heat sink thermal performance with different geometries and configurations of variable frequency air conditioner outdoor unit. To allow for interaction of heat sink and fan, both numerical and experimental investigations were done in an air conditioner outdoor unit. An increase in heat sink base area significantly improved its thermal performance; fin height and pitch influence convective surface and also sweeping stream behavior and a good compromise were needed to increase convective heat transfer. A proper tuning of heat sink configuration was effective to improve convective stream and subsequently increase thermal performance. Heat sink geometry and configuration didn’t effect very much fan aerodynamic and aeroacoustic performance, and air conditioner system performance.

When the studies about split air conditioners are investigated, it is seen that there are studies about noise level and outdoor unit positioning, mostly. The literature survey shows that there isn’t any study about modelling an outdoor unit of a split air conditioner three dimensionally by implementing CFD method. For the first time, the flow structure and axial fan performance of split air conditioner’s outdoor unit were investigated for different design parameters in this study. The outdoor unit's numerical model was analyzed under transient state condition. Furthermore, PIV was used to observe and verify flow structure of outdoor unit as an experimental method. Additionally, another experimental method was used to determine and validate mass flow rate of air, which is blown by outdoor unit's axial fan. By following the verification of numerical model, the geometrical parameters of outdoor unit were investigated parametrically for getting optimum fan performance. The results of parametric study showed that nozzle depth and diameter, fan position and heat exchanger position had significant effects on axial fan performance coefficients of outdoor unit.

CHAPTER TWO
AIR CONDITIONING SYSTEM

2.1 History of Air Conditioners Development

Modern air conditioning emerged from advances in chemistry during the 19th century, and the first large-scale electrical air conditioning was invented and used in 1902 by American inventor Willis Carrier. The introduction of residential air conditioning in the 1920s helped enable the great migration to the Sun Belt in the United States.

In 1758, Benjamin Franklin and John Hadley, a chemistry professor at Cambridge University, conducted an experiment to explore the principle of evaporation as a means to rapidly cool an object. Franklin and Hadley confirmed that evaporation of highly volatile liquids could be used to drive down the temperature of an object past the freezing point of water. They conducted their experiment with the bulb of a mercury thermometer as their object and with a bellows used to speed-up the evaporation. They lowered the temperature of the thermometer bulb down to −14 °C while the ambient temperature was 18 °C. Franklin noted that, soon after they passed the freezing point of water 0 °C, a thin film of ice formed on the surface of the thermometer's bulb and that the ice mass was about a quarter-inch thick when they stopped the experiment upon reaching −14 °C.

In 1820, English scientist and inventor Michael Faraday discovered that compressing and liquefying ammonia could chill air when the liquefied ammonia was allowed to evaporate. In 1842, Florida physician John Gorrie used compressor technology to create ice, which he used to cool air for his patients in his hospital in Apalachicola, Florida. He hoped to eventually use his ice-making machine to regulate the temperature of buildings. He even envisioned centralized air conditioning that could cool entire cities. Though his prototype leaked and performed irregularly, Gorrie was granted a patent in 1851 for his ice-making machine. His hopes for its success vanished soon afterwards when his chief financial backer died;

Gorrie did not get the money he needed to develop the machine. According to his biographer, Vivian M. Sherlock, he blamed the "Ice King", Frederic Tudor, for his failure, suspecting that Tudor had launched a smear campaign against his invention. Dr. Gorrie died impoverished in 1855, and the idea of air conditioning went away for 50 years.

In 1902, the first modern electrical air conditioning unit was invented by Willis Carrier in Buffalo, New York. After graduating from Cornell University, Carrier found a job at the Buffalo Forge Company. While there, he began experimenting with air conditioning as a way to solve an application problem for the Sackett-Wilhelms Lithographing and Publishing Company in Brooklyn, New York. The first air conditioner, designed and built in Buffalo by Carrier, began working on 17 July 1902.

Designed to improve manufacturing process control in a printing plant, Carrier's invention controlled not only temperature but also humidity. Carrier used his knowledge of the heating of objects with steam and reversed the process. Instead of sending air through hot coils, he sent it through cold coils (filled with cold water). The air was cooled, and thereby the amount of moisture in the air could be controlled, which in turn made the humidity in the room controllable. The controlled temperature and humidity helped maintain consistent paper dimensions and ink alignment. Later, Carrier's technology was applied to increase productivity in the workplace, and The Carrier Air Conditioning Company of America was formed to meet rising demand. Over time, air conditioning came to be used to improve comfort in homes and automobiles as well.

In 1906, Stuart W. Cramer of Charlotte, North Carolina was exploring ways to add moisture to the air in his textile mill. Cramer coined the term "air conditioning", using it in a patent claim he filed that year as an analogue to "water conditioning", then a well-known process for making textiles easier to process. He combined moisture with ventilation to "condition" and change the air in the factories, controlling the humidity so necessary in textile plants. Willis Carrier adopted the term and incorporated it into the name of his company.

Shortly thereafter, the first private home to have air conditioning was built in Chapel Hill, North Carolina in 1933. Realizing that air conditioning would one day be a standard feature of private homes, particularly in regions with warmer climate, David St. Pierre DuBose (1898-1994) designed a network of ductwork and vents for his home Meadowmont, all disguised behind intricate and attractive Georgian-style open mouldings. This building is believed to be one of the first private homes in the United States equipped for central air conditioning.

In 1945, Robert Sherman of Lynn, Massachusetts invented a portable, in-window air conditioner that cooled, heated, humidified, dehumidified, and filtered the air. The idea was subsequently stolen by a large manufacturer. Sherman did not have the resources to fight the big corporation in court and thus never received any money or recognition.

2.2 Refrigeration Cycle of Air Conditioning System

Air conditioners works as heat pump. While they absorb heat from inside and reject to outside in summer, they provide heat for inside and reject to cold air to outside in winter.

Working principle of air conditioning system is called *refrigeration cycle*. This cycle is called *ideal vapor-compression refrigeration cycle* under ideal conditions, but in real life it is called *actual vapor-compression refrigeration cycle.*

2.2.1 The Ideal Vapor-Compression Refrigeration Cycle

The vapor-compression refrigeration cycle is widely used for refrigerators, air conditioning systems, and heat pumps. This cycle is shown in Figure 2.1. It involves four processes:

1-2 Isentropic compression in a compressor
2-3 Constant-pressure heat rejection in a condenser
3-4 Throttling in an expansion device
4-1 Constant-pressure heat absorption in an evaporator

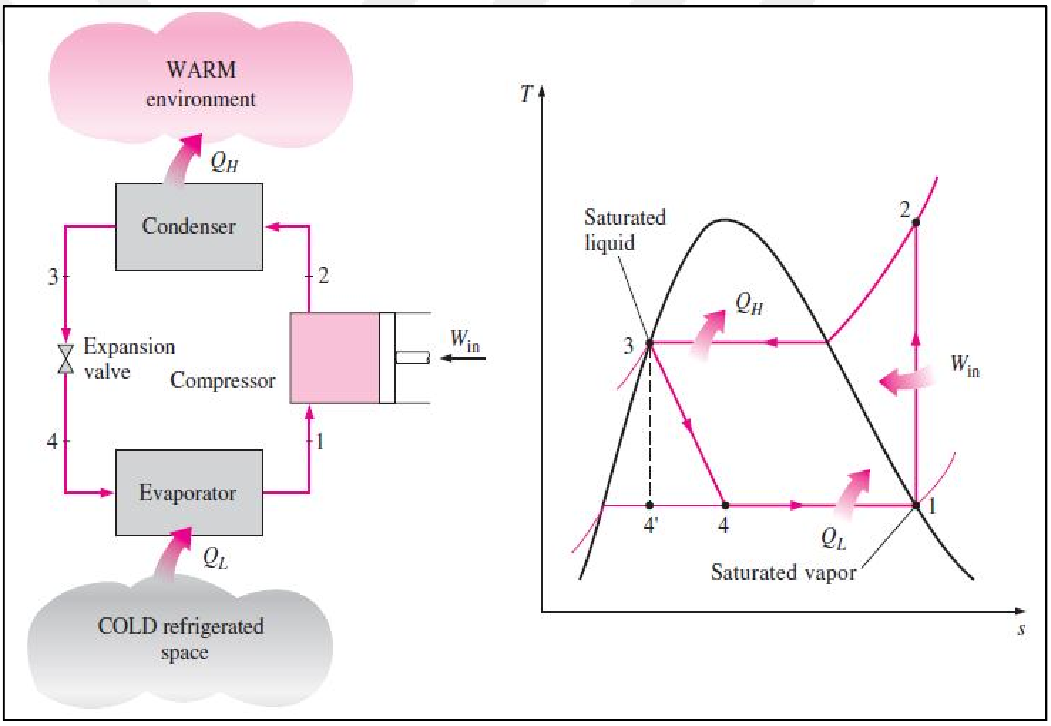

Figure 2.1 Schematic and T-s diagram for the ideal vapor-compression refrigeration cycle (Çengel & Boles, 2006)

In an ideal vapor-compression refrigeration cycle, the refrigerant enters the compressor at state 1 as saturated vapor and is compressed isentropically to the condenser pressure. The temperature of the refrigerant increases during this isentropic compression process to well above the temperature of the surrounding medium. The refrigerant then enters the condenser as superheated vapor at state 2 and leaves as saturated liquid at state 3 as a result of heat rejection to the surroundings. The temperature of the refrigerant at this state is still above the temperature of the surroundings. The saturated liquid refrigerant at state 3 is throttled to the evaporator pressure by passing it through an expansion valve or capillary tube. The temperature of the refrigerant drops below the temperature of the refrigerated space during this process. The refrigerant enters the evaporator at state 4 as a low-quality saturated mixture, and it completely evaporates by absorbing heat from the refrigerated space. The refrigerant leaves the evaporator as saturated vapor and reenters the compressor, completing the cycle (Çengel & Boles, 2006, p. 611).

The P-h diagram is the other diagram which is often used for analysis of vapour-compression refrigeration cycle. This diagram is shown in Figure 2.2. On this diagram it is seen that three of the four processes appear as straight lines, and the heat transfer in the condenser and the evaporator is proportional to the lengths of the corresponding process curves.

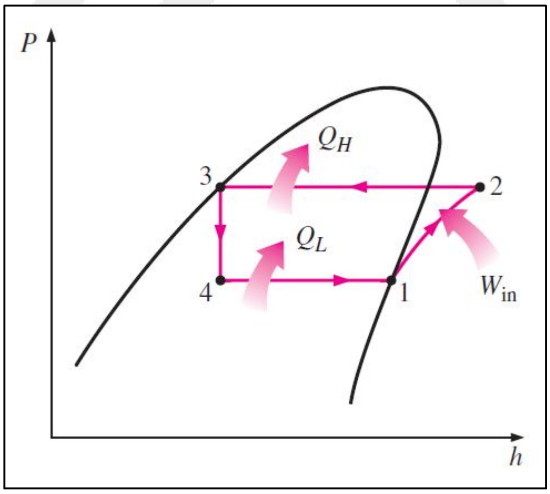

Figure 2.2 The P-h diagram of an ideal vapor-compression refrigeration cycle (Çengel & Boles, 2006)

2.2.2 The Actual Vapor-Compression Refrigeration Cycle

An actual vapor-compression refrigeration cycle is different from the ideal one in several ways, due to the irreversibilities that occur in various components. Two common sources of irreversibilities are heat transfer to or from the surroundings and fluid friction (causes pressure drops). The T-s diagram of an actual vapor-compression refrigeration cycle is shown in Figure 2.3.

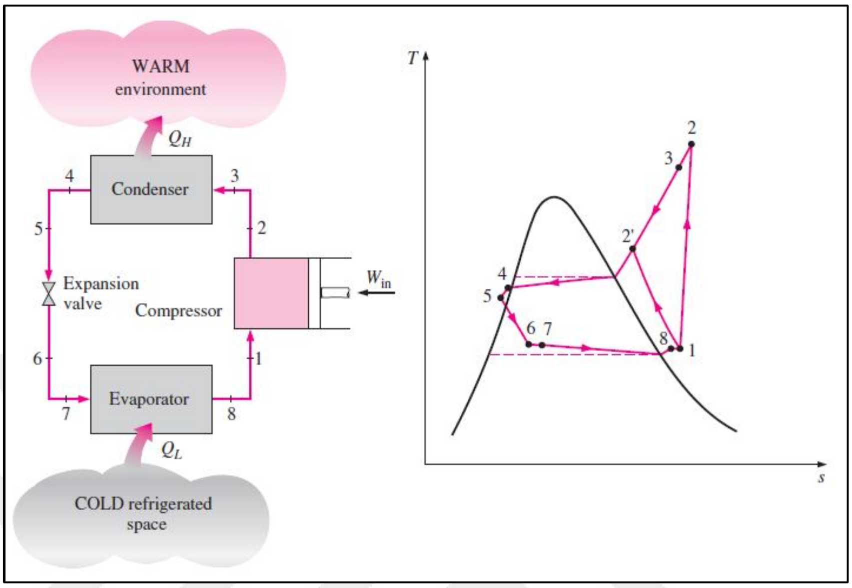

Figure 2.3 Schematic and T-s diagram for the actual vapor-compression refrigeration cycle (Çengel & Boles, 2006)

In the ideal cycle, the refrigerant leaves the evaporator and enters the compressor as saturated vapor. In practice, however, it may not be possible to control the state of the refrigerant so precisely. Instead, it is easier to design the system so that the refrigerant is slightly superheated at the compressor inlet. This slight overdesign ensures that the refrigerant is completely vaporized when it enters the compressor. Also, the line connecting the evaporator to the compressor is usually very long; thus the pressure drop caused by fluid friction and heat transfer from the surroundings to the refrigerant can be very significant. The result of superheating, heat gain in the connecting line, and pressure drops in the evaporator and the connecting line is an increase in the specific volume, thus an increase in the power input requirements to the compressor since steady-flow work is proportional to the specific volume (Çengel & Boles, 2006, p. 614).

The compression process in the ideal cycle is internally reversible and adiabatic, and thus isentropic. The actual compression process, however, includes frictional effects, which increase the entropy, and heat transfer, which may increase or decrease the entropy, depending on the direction. Therefore, the entropy of the refrigerant may increase (process 1-2) or decrease (process 1-2') during an actual compression process, depending on which effects dominate. The compression process 1-2' may be even more desirable than the isentropic compression process since the specific volume of the refrigerant and thus the work input requirement are smaller in this case. Therefore, the refrigerant should be cooled during the compression process whenever it is practical and economical to do so.

In the ideal case, the refrigerant is assumed to leave the condenser as saturated liquid at the compressor exit pressure. In real life, however, it is unavoidable to have some pressure drop in the condenser as well as in the lines connecting the condenser to the compressor and to the throttling valve. Also, it is not easy to execute the condensation process with such precision that the refrigerant is a saturated liquid at the end, and it is undesirable to route the refrigerant to the throttling valve before the refrigerant is completely condensed. Therefore, the refrigerant is subcooled somewhat before it enters the throttling valve. We do not mind this at all, however, since the refrigerant in this case enters the evaporator with a lower enthalpy and thus can absorb more heat from the refrigerated space. The throttling valve and the evaporator are usually located very close to each other, so the pressure drop in the connecting line is small.

2.3 Refrigerants

2.3.1 Refrigerant Types and Characteristics

Prior to the 1930s, accidents were prevalent among those who worked closely with refrigerants due to the toxicity and flammability of most refrigerants at the time. Because of such hazards, two classes of synthetic refrigerants were developed, each containing chlorine and possessing highly stable molecular structures: CFCs (chlorofluorocarbons) and HCFCs (hydrochlorofluorocarbons). These refrigerants were widely known as “freons,” the common trade name.

In the early 1930s, CFC production began with R-11, R-12, R-113, and R-114. In 1936, the first HCFC refrigerant, R-22, was introduced. Over the next several decades, nearly all of the synthetic refrigerants used in the United States were either CFCs or HCFCs, with R-12 being most commonly used.

To keep order with so many new refrigerants having complicated names, the "R" numbering system was established in 1956 by DuPont and persists today as the industry standard.

> After decades of use, compelling scientific data indicating that release of chlorine containing refrigerants into the atmosphere is harmful became widely recognized. Concerns focused on released refrigerants depleting the stratospheric ozone layer and contributing to global climate change. Because of the molecular stability of the CFC and HCFC molecules, their adverse effects are long-lasting. In 1987, an international agreement was adopted to ban production of certain chlorine-containing refrigerants. In response, a new class of chlorine-free refrigerants was developed: the HFCs (hydrofluorocarbons). One of these, R-134a, has been used for over 20 years as the primary replacement for R-12. Although R-134a and other HFC refrigerants do not contribute to atmospheric ozone depletion, they do contribute to global climate change (Moran, Shapiro, Boettner, & Bailey, 2014, p. 621).

Another refrigerant that has been used extensively in air-conditioning and refrigeration systems for decades, R-22, is being phased out under a 1995 amendment to the international agreement on refrigerants because of its chlorine content. Effective in 2010, R-22 cannot be installed in new systems. However, recovered and recycled R-22 can be used to service existing systems until supplies are no longer available. As R-22 is phased out, replacement refrigerants are being introduced, including R-410A and R-407C, both HFC blends.

2.3.2 Natural Refrigerants

Nonsynthetic, naturally occurring substances also can be used as refrigerants. Called natural refrigerants, they include carbon dioxide, ammonia, and hydrocarbons.

Ammonia (R-717), which was widely used in the early development of vapour compression refrigeration, continues to serve today as a refrigerant for large systems used by the food industry and in other industrial applications. In the past two decades, ammonia has been increasingly used because of the R-12 phaseout and is receiving even greater interest today due to the R-22 phaseout.

> Hydrocarbons, such as propane (R-290), are used worldwide in various refrigeration and air-conditioning applications including commercial and household appliances. In the United States, safety concerns limit propane use to niche markets like industrial process refrigeration. Other hydrocarbons - methane (R-50) and butane (R-600) - are also under consideration for use as refrigerants (Moran, Shapiro, Boettner, & Bailey, 2014, p. 622).

2.4 Split-System Air Conditioning

Split type air conditioners consist of two units. These are indoor unit and outdoor unit. An example is shown in Figure 2.4.

Figure 2.4 Indoor and outdoor units of a split air conditioner (Air conditioner, 2016)

This air conditioning system works according to a principle which uses *Refrigeration Cycle*. Working principle of a split type air conditioner is shown in Figure 2.5.

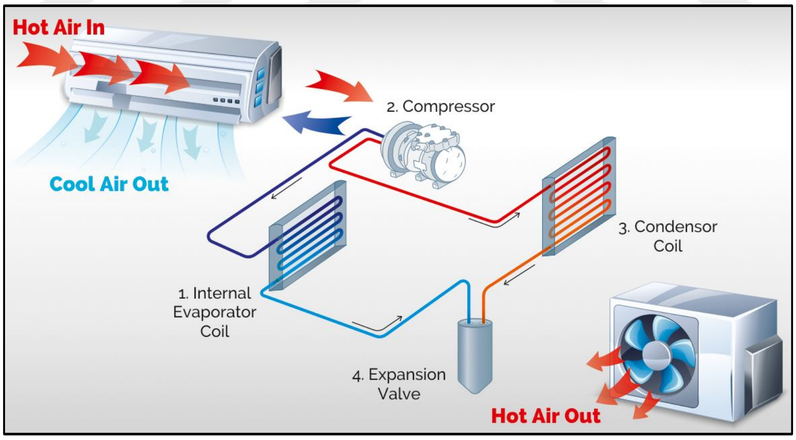

Figure 2.5 Working principle of a split air conditioner (Air conditioner, 2016)

2.4.1 Evaporation

Evaporation is the first step in removing heat energy from an indoor environment. Warm air from inside is blown across the evaporator coil by a fan, while the pipes comprising the coil are supplied with cold liquid refrigerant. When the warm indoor air passes through the cold evaporator coil, it is cooled and this cool air is delivered back to the indoor environment. Even though the evaporator coil is cold, the refrigerant inside is evaporating, or boiling, changing from liquid to gas. It is the heat from the inside environment that is making the refrigerant boil, passing heat energy to the refrigerant in the process. The refrigerant at this point is a cool gas in a small pipe that is carrying the heat energy away from inside environment.

2.4.2 Compression

The vaporized but cool refrigerant carrying the heat from inside environment is drawn into a compressor. This compressor has two important functions:

1. It pushes the refrigerant carrying the heat energy around the refrigeration loop.
2. It compresses the gas refrigerant from the evaporator coil.

It is a fundamental property of gases that the compression of a gas causes its measured temperature to rise. Therefore, the moving gas refrigerant exiting the compressor is hot, as well as compressed. This temperature rise due to compression is the key to the ability of the refrigeration loop to eject heat into the outdoor environment.

2.4.3 Condensation

The hot compressed refrigerant carries the inside environment heat energy from the compressor to the condenser coil. Like the evaporator coil, this coil transfers heat to another medium, like air. But unlike the evaporator coil which was has lower temperature than the air flowing across the coil, the condenser coil operates at a higher temperature than the air. This means that the air flowing across the coil is heated by the coil, and that the hot gas refrigerant flowing through the coil is conversely cooled. Heat is flowing from the refrigerant to the air. The air is typically blown across the hot coil by a fan which exhausts the hot air to the outdoor environment. In this way, heat energy from inside environment has been pumped outdoor environment.

2.4.4 Expansion

The refrigerant exits the condenser coil as a hot, high-pressure liquid. The refrigerant is then piped to a device called an expansion valve positioned at the entrance to the evaporator coil. This valve has two key functions that are critical for refrigeration cycle:

1. It precisely regulates the flow of high-pressure refrigerant into the low-pressure evaporator coil at a rate that maintains an optimal difference in pressure to ensure all refrigerant is evaporated prior to leaving the coil.
2. The refrigerant again becomes capable of being expanded (boiled) to a gas by the heat energy in the data center as it escapes the expansion valve and re-enters the evaporator coil.

In this way the refrigeration cycle is repeated, and the net result of the process is that heat is continuously flowing into the evaporator coil and continuously flowing out of the condenser coil. An air conditioner system operated in this way will continuously pump heat energy out of the inside environment.

CHAPTER THREE
COMPONENTS OF AN OUTDOOR UNIT OF A SPLIT AIR CONDITIONER

3.1 Axial Fan

Room air conditioners typically consist of a single motor driving two fans, the condenser and evaporator blower fans. A variety of fan types can be used in room air conditioners, as illustrated in Figure 3.1.

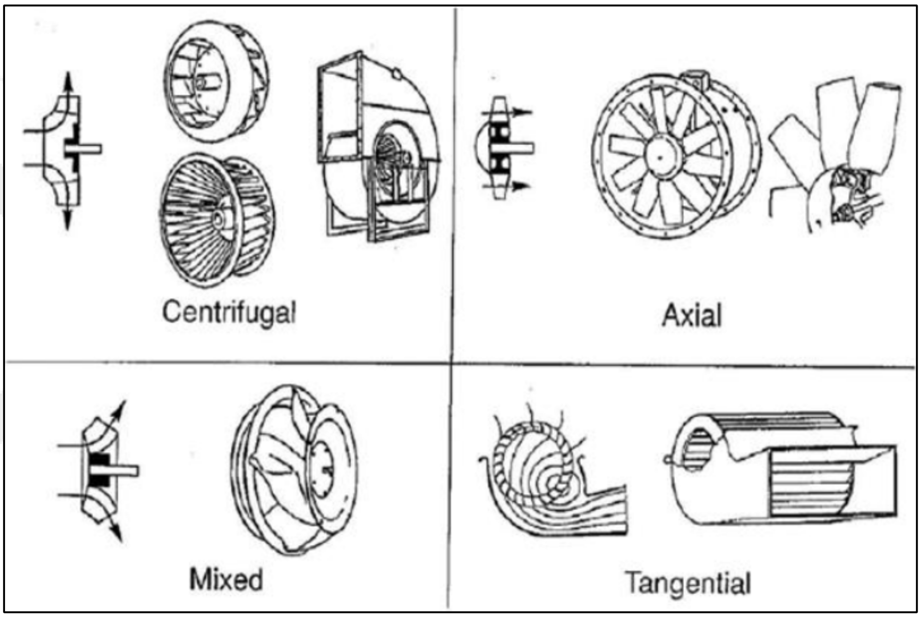

Figure 3.1 Types of different fans (Cooling the planet: opportunities for deployment of superefficient room air conditioners, 2013)

Cross-flow fans or centrifugal fans are used to produce forced air flow for indoor units, whereas axial fans tend to be used in the outdoor units. Variable speed electrical motors are used to drive these fans in order to adjust the air flow rate as required by the end-users. The type of fans used for split and multisplit systems varies for these indoor units, however, most of the outdoor fan units tend to be of the axial variety. Window or wall units tend to use centrifugal fans for both sides. Whereas, in the case of single and double duct systems a single fan (centrifugal) is used for both the condenser and evaporator coils. Mobile split units use centrifugal fans indoor and axial fans for the outdoor. Any design improvements in the fan which seek to improve the air flow characteristics can have a marked reduction in power demand from the fan motor and thus increase the overall efficiency. It is important to note, however, that any design changes to improve air flow must be developed in the context of space limitations of in-room air conditioners and that any design changes in the heat exchanger may lead to alterations in the air flow.

The efficiency of propeller fans has improved significantly. Older versions were made of processed metals, whereas plastics are now used in the more efficient models. The shape has also progressively evolved in order to increase the volumetric efficiency and achieve a reduced noise level. This evolutionary process moving from a 2D wing in the mid/late 1970s to a hybrid wing design in the late 1990s/early 2000s is summarized by Figure 3.2.

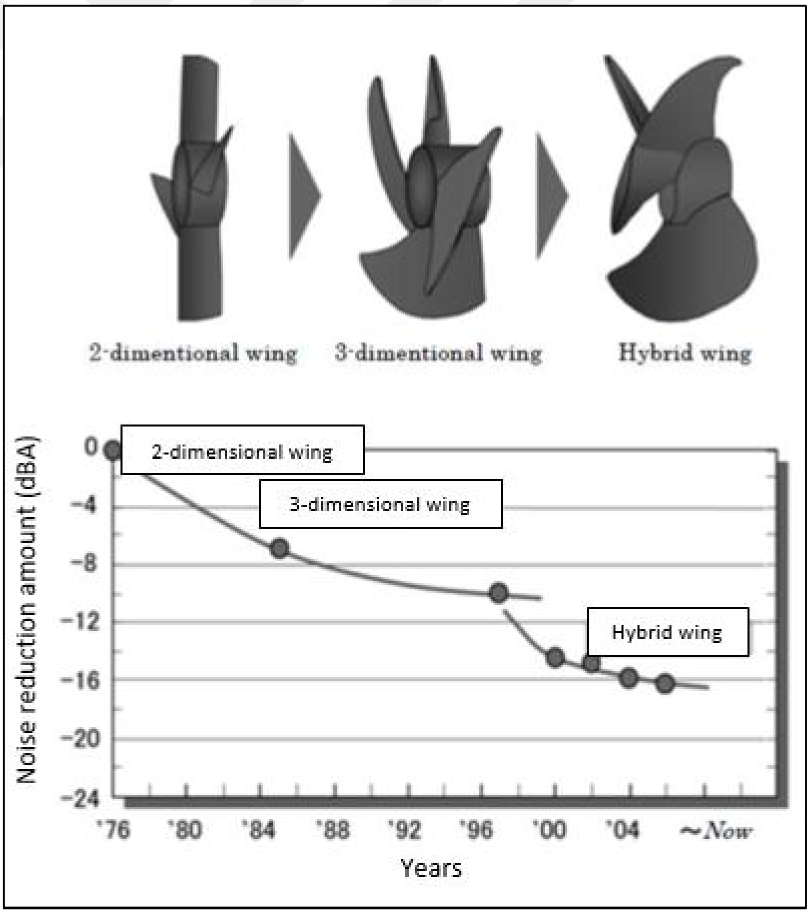

Figure 3.2 Fan evolution of axial/propeller fan design (Cooling the planet: opportunities for deployment of superefficient room air conditioners, 2013)

3.1.1 Types of Axial Fans

The main types of axial flow fans (propeller, tube-axial and vane-axial) are summarized in Table 3.1.

Table 3.1 Types of axial fans

Type	Characteristics	Applications
Propeller Fans	- develop high airflow rates and low pressures - not suitable for extensive ductwork - relatively low efficiencies - inexpensive - comparatively noisy - power requirements of propeller fans decrease with increasing airflow - maximum efficiency at lowest delivery pressure	- often used in rooftop ventilation applications
Tube-axial Fans	- achieve higher pressures and better operating efficiencies than propeller fans - applied in medium-pressure, high air flow rate applications - the airflow downstream of the fan is uneven, with a large rotational component - generates moderate airflow noise - because of low rotating mass, they can quickly accelerate to rated speed - because of the high operating speeds of 2-, 4-, and 6-pole induction motors, most tube-axial fans use belt drives to achieve - fan speeds below 1,100 revolutions per minute	- well-suited for ducted HVAC installations - ventilation applications
Vane-axial Fans	- a vaneaxial fan is essentially a tubeaxial fan with outlet vanes to straighten the airflow, converting the airstream's kinetic energy to static pressure - the airflow profile is uniform - when equipped with variable pitch blades, can be adjusted to change the angle of attack to the incoming air stream and air delivery rate - have unstable regions to the left of the peak pressure - highly efficient: when equipped with airfoil blades and built with small clearances, efficiencies up to 85 percent are achievable	- typically used in medium- to highpressure applications, such as induced draft service for a boiler exhaust - low rotating mass, which allows them to achieve operating speed relatively quickly

The performance curve for propeller fans is shown in Figure 3.3.

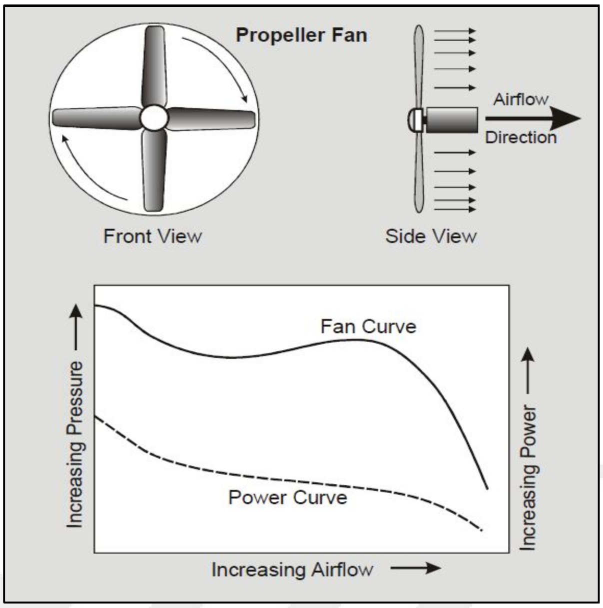

Figure 3.3 Propeller fan (Energy efficiency reference guide: Fans and blowers, 2016)

The performance curve for tube-axial fans is shown in Figure 3.4.

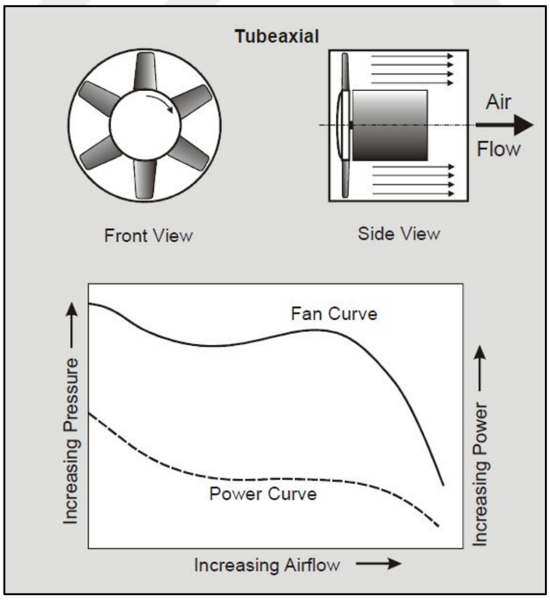

Figure 3.4 Tube axial fan (Energy efficiency reference guide: Fans and blowers, 2016)

The performance curve for vane-axial fans is shown in Figure 3.5.

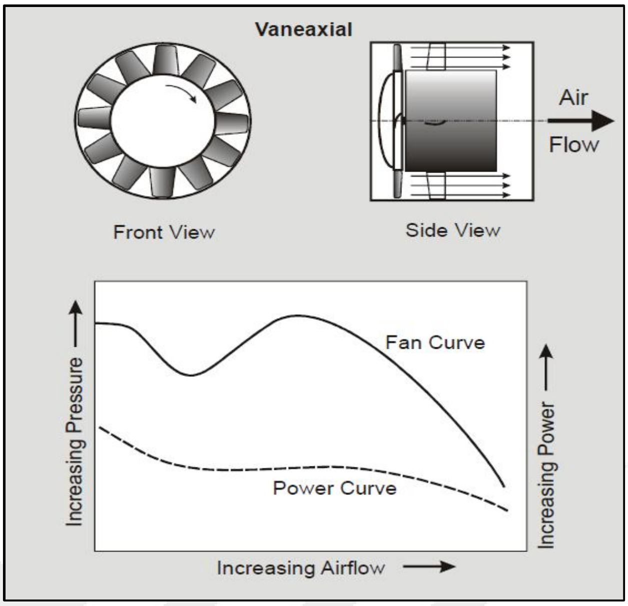

Figure 3.5 Vane axial fan (Energy efficiency reference guide: Fans and blowers, 2016)

3.2 Compressor

Compressors make heat transfer happen from cold environment to hot environment by pumping the refrigerant in split air conditioner. This means that compressors suck cooling refrigerant, which is at vapor state and has lower pressure, from evaporator and send it to condenser, which has higher pressure.

There are five main types of split air conditioner compressors:

- Rotary Compressors
- Reciprocating Compressors
- Screw Compressors
- Centrifugal Compressor
- Scroll Compressors

Typically the use of scroll and rotary compressors are likely to be used in the cooling capacity range required by residential air conditioners. In the rotary compressor it is the rotating action of the roller inside the cylinder which compresses the refrigerant. The capacity of the scroll compressor ranges from one to twenty horse power. It uses a stationary and orbiting scroll which compresses the refrigerant gas vapors between the evaporator and the condenser. The cooling capacity of reciprocating compressors ranges from one to several hundred horsepower. They work best when they are used with refrigerants that call for relatively small displacement and condensing at high pressures.

The relative efficiency advantage of scroll, rotary and displacement compressor technology depends on the desired cooling capacity. Rotary compressors are the most common types of compressor for low capacity units (below 6 kW) and multi-split air conditioners. For larger capacity units, scroll compressors are often used, alongside reciprocating (displacement) compressors. Since 1965 scroll compressor efficiency, when expressed as the fraction of the isentropic efficiency, rose from 0.48 to 0.73 in 2002. The rate of improvement, however, is slowing and only more modest additional improvements are expected in the future. The total "heat insulated" efficiency of scroll compressors, i.e. the ratio between the work supplied to the fluid and the electric power delivered by the motor of the compressor, reached 80% in 2004. Thus when coupled with a high efficiency motor, overall compressor efficiencies of about 75% are currently attained. The energy efficiency of rotary compressors has also continued to improve especially through the reduction in friction losses and by minimizing leakage between the high and low pressure sides. Some Japanese manufacturers have adopted rotary compressors with two stages, i.e. using twin rotary compression that has increased compressor efficiency by ~10%. The use of very high efficiency DC motors with optimized scroll compressors is another high efficiency solution.

3.3 Condenser

A condenser gives cooling refrigerant's heat to the outdoor envirionment by condensing cooling refrigerant, which is at superheated vapor state and has high pressure and temperature.

Condensers are classified as air-cooled condenser and water-cooled condenser according to how it rejects the heat.

3.3.1 Air-Cooled Condenser

These condensers are used for conditions in which maximum 750 W cooling capacity is required. They are preferred for simplicity, low installation and operating costs. They are usually manufactured as finned and tube heat exchanger. The cooling refrigerant flows inside tubes and the air flows along outer surfaces of tubes.

3.3.2 Water-Cooled Condenser

Water is used for cooling in water-cooled condensers. Water-cooled condensers have more common usage in comercial and industrial cooling systems than air-cooled condensers because they are smaller than air-cooled condensers when both of them have the same capacity.

A water-cooled condenser has lower condensing temperature because water has lower temperature than surrounding temperature. Therfore a compressor, which is used in a water-cooled condenser, requires lower horse power.

CHAPTER FOUR
COMPUTATIONAL FLUID DYNAMICS

4.1 History of Computational Fluid Dynamics

The history of Computational Fluid Dynamics, or CFD for short, started in the early 1970's. Around that time, it became an acronym for a combination of physics, numerical mathematics, and, to some extent, computer sciences employed to simulate fluid flows. The beginning of CFD was triggered by the availability of increasingly more powerful mainframes and the advances in CFD are still tightly coupled to the evolution of computer technology. Among the first applications of the CFD methods was the simulation of transonic flows based on .the solution of the non-linear potential equation. With the beginning of the 1980's, the solution of first two-dimensional (2-D) and later also three-dimensional (3-D) Euler equations became feasible. Thanks to the rapidly increasing speed of supercomputers and due to the development of a variety of numerical acceleration techniques like multigrid, it was possible to compute inviscid flows past complete aircraft configurations or inside of turbomachines. With the mid 1980's, the focus started to shift to the significantly more demanding simulation of viscous flows governed by the Navier-Stokes equations. Together with this, a variety of turbulence models evolved with different degree of numerical complexity and accuracy. The leading edge in turbulence modelling is represented by the Direct Numerical Simulation (DNS) and the Large Eddy Simulation (LES). However, both approaches are still far away from being usable in engineering applications (Blazek, 2001, p. 1).

Nowadays, CFD methodologies are routinely employed in the fields of aircraft, turbomachinery, car, and ship design. Furthermore, CFD is also applied in meteorology, oceanography, astrophysics, in oil recovery, and also in architecture. Many numerical techniques developed for CFD are used in the solution of Maxwell equations as well. Hence, CFD is becoming an increasingly important design tool in engineering and also a substantial research tool in certain physical sciences. Due to the advances in numerical solution methods and computer technology, geometrically complex cases, like those which are often encountered in turbomachinery, can be treated. Also, large scale simulations of viscous flows can be accomplished within only a few hours on today's supercomputers, even for grids consisting of dozens of millions of grid cells. However, it would be completely wrong to think that CFD represents a mature technology now, like for example structural finite element methods. No, there are still many open questions like turbulence and combustion modelling, heat transfer, efficient solution techniques for viscous flows, robust but accurate discretisation methods, etc. Also the connection of CFD with other disciplines (like structural mechanics or heat conduction) requires further research. Quite new opportunities also arise in the design optimisation by using CFD.

4.2 Mathematical Description of Flow

The derivation of the principal equations of fluid dynamics is based on the fact that the dynamical behaviour of a fluid is determined by the following conservation laws, namely:

1. the conservation of mass,
2. the conservation of momentum, and
3. the conservation of energy.

4.2.1 Finite Volume Control

An arbitrary finite region of the flow, bounded by the closed surface $\partial\Omega$ and fixed in space, defines the control volume Ω. We also introduce a surface element as dS and its associated, outward pointing unit normal vector as $\vec{n}$.

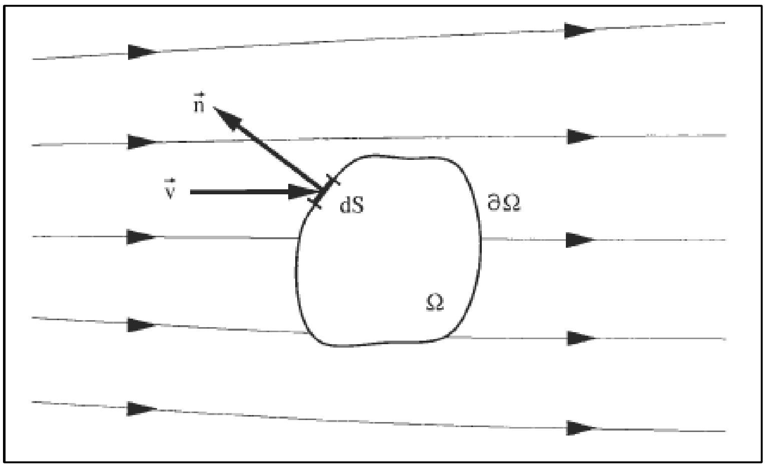

Figure 4.1 Definition of a control volume (fixed in space) (Blazek, 2001)

The conservation law applied to an exemplary scalar quantity per unit volume *U* now says that its variation in time within **Ω**, i.e.,

$$\frac{\partial}{\partial t}\int_{\Omega} U \, d\Omega \tag{4.1}$$

is equal to the sum of the contributions due to the convective flux – amount of the quantity U entering the control volume through the boundary with the velocity $\vec{v}$ – hence $U\vec{v}$

$$-\oint_{\partial\Omega} U(\vec{v}.\vec{n})dS \tag{4.2}$$

due to the diffusive flux - expressed by the generalised Fick's gradient law

$$\oint_{\partial\Omega} \kappa\rho[\nabla(U/\rho).\vec{n}]dS \tag{4.3}$$

where **κ** is the thermal diffusivity coefficient, and due to the volume as well as surface sources, Q_V, $\overrightarrow{Qs}$, i.e.,

$$\int_{\Omega} Q_V d\Omega + \oint_{\partial\Omega}(\overrightarrow{Qs}.\vec{n})dS \tag{4.4}$$

respectively. After summing the above contributions, we obtain the following general form of the conservation law for the scalar quantity *U*

$$\frac{\partial}{\partial t}\int_{\Omega} U \, d\Omega + \frac{\partial}{\partial t}\int_{\Omega} U \, d\Omega = \int_{\Omega} Q_V d\Omega + \oint_{\partial\Omega}(\overrightarrow{Qs}.\vec{n})dS \tag{4.5}$$

where U*denotes the quantity U per unit mass, i.e., U/ρ.

It is important to note that if the conserved quantity would be a vector instead of a scalar, the above Equation (4.5) would formally still be valid. But in difference, the convective and the diffusive flux would become tensors instead of vectors - $\overline{\overline{F_C}}$ the convective flux tensor and $\overline{\overline{F_D}}$ the diffusive flux tensor. The volume sources would be a vector, $\overrightarrow{Q_V}$, and the surface sources would change into a tensor $\overline{\overline{Q_S}}$. We can therefore write the conservation law for a general vector quantity $\vec{U}$ as

$$\frac{\partial}{\partial t}\int_{\Omega} \vec{U} \, d\Omega + \oint_{\partial\Omega}[(\overline{\overline{F_C}} - \overline{\overline{F_D}}).\vec{n}]dS = \int_{\Omega} \overrightarrow{Q_V} d\Omega + \oint_{\partial\Omega}(\overline{\overline{Q_S}}.\vec{n})dS \tag{4.6}$$

The integral formulation of the conservation law, as given by the Equations (4.5) or (4.6), has two very important and desirable properties:

1. if there are no volume sources present, the variation of U depends solely on the flux across the boundary $\partial\Omega$ and not on any flux inside the control volume Ω;
2. this particular form remain valid in the presence of discontinuities in the flow field like shocks or contact discontinuities.

Because of its generality and its desirable properties, it is not surprising that the majority of CFD codes is based today on the integral form of the governing equations.

4.3 Conversation Laws

4.3.1 The Continuity Equation

In order to derive the continuity equation, the model of a finite control volume fixed in space is utilized as sketched in Fig. 4.1. At a point on the control surface, the flow velocity is $\vec{v}$, the unit normal vector is $\vec{n}$ and dS denotes an elemental surface area. The conserved quantity in this case is the density ρ. For the time rate of change of the total mass inside the finite volume **Ω**, there is

$$\frac{\partial}{\partial t}\int_{\Omega} \rho \, d\Omega \qquad (4.7)$$

The mass flow of a fluid through some surface fixed in space equals to the product of (density) x (surface area) x (velocity component perpendicular to the surface). Therefore, the contribution from the convective flux across each surface element *dS* becomes

$$\rho(\vec{v}.\vec{n})\mathrm{dS} \qquad (4.8)$$

Since by convection $\vec{n}$ always points out of the control volume, it can be mentioned of inflow if the product $(\vec{v}.\vec{n})$ is negative, and of *outflow* if it is positive and hence the mass flow leaves the control volume. As stated above, there are no volume or surface sources present. Thus, by taking into account the general formulation of Eq. (4.5), it can be written

$$\frac{\partial}{\partial t}\int_{\Omega} \rho \, d\Omega + \oint_{\partial\Omega} \rho(\vec{v}.\vec{n})\mathrm{dS} = 0 \qquad (4.9)$$

This represents the integral form of the continuity equation - the conservation law of mass.

4.3.2 The Momentum Equation

The momentum equation can be derived by recalling the particular form of Newton's second law which states that the variation of momentum is caused by the net force acting on a mass element. For the momentum of an infinitesimally small portion of the control volume **Ω** (see Fig. 4.1) we have

$$\rho\vec{v}\, d\Omega \tag{4.10}$$

The variation in time of momentum within the control volume equals

$$\frac{\partial}{\partial t}\int_{\Omega} \rho\vec{v}\, d\Omega \tag{4.11}$$

Hence, the conserved quantity is here the product of density times the velocity, i.e.,

$$\rho\vec{v} = [\ \rho u, \rho v, \rho w\ ]^{T} \tag{4.12}$$

The convective flux tensor, which describes the transfer of momentum across the boundary of the control volume, consists in the Cartesian coordinate system of the following three components

x-component : $\rho u\, \vec{v}$

y-component : $\rho v\, \vec{v}$

z-component : $\rho w\, \vec{v}$

The contribution of the convective flux tensor to the conservation of momentum is then given by

$$\oint_{\partial\Omega} \rho\vec{v}.\,(\vec{v}.\vec{n})dS \tag{4.13}$$

The diffusive flux is zero, since there is no diffusion of momentum possible for a fluid at rest. Two kinds of forces acting on the control volume can be identified like:

1. External volume or body forces, which act directly on the mass of the volume. These are for example gravitational, buoyancy, Coriolis or centrifugal forces. In some cases, there can be electromagnetic forces present as well.

2. Surface forces, which act directly on the surface of the control volume. They result from only two sources:

(a) the pressure distribution, imposed by the outside fluid surrounding

(b) the shear and normal stresses, resulting from the friction between the fluid and the surface of the volume.

From the above, it can be seen that the body force per unit volume, denoted as $\rho\vec{f_e}$, corresponds to the volume sources in Eq. (4.5). Thus, the contribution of the body (external) force to the momentum conservation is

$$\int_{\Omega} \rho\vec{f_e}\, d\Omega \tag{4.14}$$

The surface sources consist then of two parts - an isotropic pressure component and a viscous stress tensor $\bar{\bar{\tau}}$, i.e.,

$$\bar{\bar{Q}}s = -p\bar{\bar{I}} + \bar{\bar{\tau}} \tag{4.15}$$

with $\bar{\bar{I}}$ being the unit tensor. The effect of the surface sources on the control volume is sketched in Fig. 4.2.

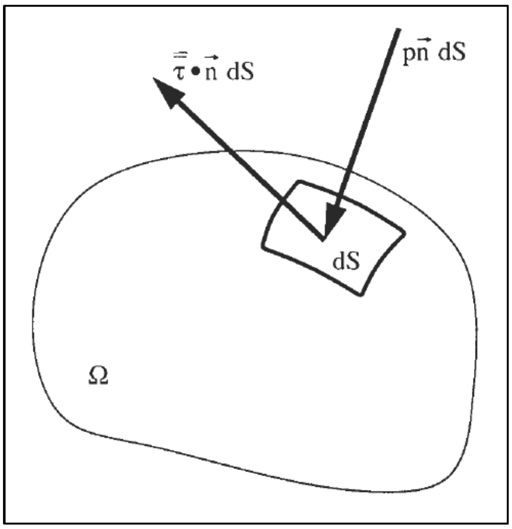

Figure 4.2 Surface forces acting on a surface element of the control volume (Blazek, 2001)

If all the above contributions according to the general conservation law is summed up (Eq. (4.6)), it is finally obtain the expression

$$\frac{\partial}{\partial t}\int_{\Omega}\rho\vec{v}\, d\Omega + \oint_{\partial\Omega}\rho\vec{v}.\,(\vec{v}.\vec{n})dS = \int_{\Omega}\rho\vec{f_e}\, d\Omega - \oint_{\partial\Omega} p\vec{n}\, dS + \oint_{\partial\Omega}(\bar{\bar{\tau}}.\vec{n})\, dS \qquad (4.16)$$

for the momentum conservation inside an arbitrary control volume Ω which is fixed in space.

4.3.3 The Energy Equation

The underlying principle that it will be applied in the derivation of the energy equation, is the first law of thermodynamics. Applied to the control volume displayed in Fig. 4.1, it states that any changes in time of the total energy inside the volume are caused by the rate of work of forces acting on the volume and by the net heat flux into it. The total energy per unit mass E of a fluid is obtained by adding its internal energy per unit mass, *e,* to its kinetic energy per unit mass, $|\vec{v}|^2$ / 2. Thus, it can be written for the total energy

$$E = e + \frac{|\vec{v}|^2}{2} + \frac{u^2 + v^2 + w^2}{2} \qquad (4.17)$$

The conserved quantity is in this case the total energy per unit volume, i.e., ρE. Its variation in time within the volume Ω can be expressed as

$$\frac{\partial}{\partial t}\int_{\Omega} \rho E \, d\Omega \tag{4.18}$$

Following the discussion in course of the derivation of the general conservation law (Eq. (4.5)), it can be readily specified the contribution of the convective flux as

$$\oint_{\partial\Omega} \rho E \, (\vec{v}.\vec{n}) \, dS \tag{4.19}$$

In contrast to the continuity and the momentum equation, there is now a diffusive flux. It is proportional to the gradient of the conserved quantity per unit mass (Fick's law). Since the diffusive flux $\overrightarrow{F_D}$ is defined for fluid at rest, only the internal energy becomes effective and it is obtained

$$\overrightarrow{F_D} = -\gamma \, \rho \, \kappa \, \nabla \, e \tag{4.20}$$

In the above, $\gamma = \frac{c_p}{c_v}$ is the ratio of specific heat coefficients, and κ denotes the thermal diffusivity coefficient. The diffusion flux represents one part of the heat flux into the control volume, namely the diffusion of heat due to molecular thermal conduction - heat transfer due to temperature gradients. Therefore, Equation (4.20) is in general written in the form of Fourier's law of heat conduction, i.e.,

$$\overrightarrow{F_D} = -k \, \nabla \, T \tag{4.21}$$

with k standing for the thermal conductivity coefficient and T for the absolute static temperature.

The other part of the net heat flux into the finite control volume consists of volumetric heating due to absorption or emission of radiation, or due to chemical reactions. We will denote the heat sources - the time rate of heat transfer per unit mass - as $\dot{q}_h$. Together with the rate of work done by the body forces $\vec{f_e}$, which we have introduced for the momentum equation, it completes the volume sources

$$Q_V = \rho\vec{f_e}.\vec{v} + \dot{q}_h \tag{4.22}$$

The last contribution to the conservation of energy, which we have yet to determine, are the surface sources Q_S. They correspond to the time rate of work done by the pressure as well as the shear and normal stresses on the fluid element

$$\overrightarrow{Q_S} = -p\vec{v} + \bar{\bar{\tau}}.\vec{v} \tag{4.23}$$

Sorting now all the above contributions and terms, we obtain for the energy conservation equation the expression

$$\frac{\partial}{\partial t}\int_\Omega \rho E\, d\Omega + \oint_{\partial\Omega} \rho E\,(\vec{v}.\vec{n})\, dS = \oint_{\partial\Omega} k\,(\nabla T.\vec{n})\, dS + \int_\Omega (\rho\vec{f_e}.\vec{v} + \dot{q}_h)\, d\Omega$$
$$- \oint_{\partial\Omega} p(\vec{v}.\vec{n})\, dS + \oint_{\partial\Omega} (\bar{\bar{\tau}}.\vec{v}).\vec{n}\, dS \tag{4.24}$$

Usually, the energy equation (4.24) is written in a slightly different form. For that purpose, it will be utilised the following general relation between the total enthalpy, the total energy and the pressure

$$H = h + \frac{|\vec{v}|^2}{2} = E + \frac{p}{\rho} \tag{4.25}$$

When it is gathered the convective ($\rho E\vec{v}$) and the pressure term ($p\vec{v}$) in the energy conservation law (4.24) and apply the formula (4.25), it can be finally written the energy equation in the form

$$\frac{\partial}{\partial t}\int_\Omega \rho E\, d\Omega + \oint_{\partial\Omega} \rho H\,(\vec{v}.\vec{n})\, dS = \oint_{\partial\Omega} k\,(\nabla T.\vec{n})\, dS + \int_\Omega (\rho\vec{f_e}.\vec{v} + \dot{q}_h)\, d\Omega$$
$$+ \oint_{\partial\Omega} (\bar{\bar{\tau}}.\vec{v}).\vec{n}\, dS \tag{4.26}$$

Herewith, we have derived integral formulations of the three conservation laws: the conservation of mass (4.9), of momentum (4.16), and of energy (4.26).

CHAPTER FIVE
PARTICLE IMAGE VELOCIMETRY

5.1 Introduction to Particle Image Velocimetry

Particle image velocimetry (PIV) is an optical method of flow visualization used in education and research. It is used to obtain instantaneous velocity measurements and related properties in fluids. The fluid is seeded with tracer particles which, for sufficiently small particles, are assumed to faithfully follow the flow dynamics. The fluid with entrained particles is illuminated so that particles are visible. The motion of the seeding particles is used to calculate speed and direction (the velocity field) of the flow being studied.

Other techniques used to measure flows are laser Doppler velocimetry and hot-wire anemometry. The main difference between PIV and those techniques is that PIV produces two-dimensional or even three-dimensional vector fields, while the other techniques measure the velocity at a point. During PIV, the particle concentration is such that it is possible to identify individual particles in an image, but not with certainty to track it between images. When the particle concentration is so low that it is possible to follow an individual particle it is called Particle tracking velocimetry, while Laser speckle velocimetry is used for cases where the particle concentration is so high that it is difficult to observe individual particles in an image.

While the method of adding particles or objects to a fluid in order to observe its flow is likely to have been used from time to time through the ages no sustained application of the method is known. The first to use particles to study fluids in a more systematic manner was Ludwig Prandtl, in the early 20th century.

Laser Doppler Velocimetry predates PIV as a laser-digital analysis system to become widespread for research and industrial use. Able to obtain all of a fluid's velocity measurements at a specific point, it can be considered the 2-dimensional PIV's immediate predecessor. PIV itself found its roots in Laser speckle velocimetry, a technique that several groups began experimenting with in the late 1970s. In the early 1980s it was found that it was advantageous to decrease the particle concentration down to levels where individual particles could be observed. At these particle densities it was further noticed that it was easier to study the flows if they were split into many very small 'interrogation' areas, that could be analyzed individually to generate one velocity for each area. The images were usually recorded using analog cameras and needed immense amount of computing power to be analyzed.

With the increasing power of computers and widespread use of CCD cameras, digital PIV has become increasingly common, to the point that it is the primary technique today.

5.2 System Components for PIV

Typical PIV apparatus consists of a camera (normally a digital camera with a CCD chip in modern systems), a strobe or laser with an optical arrangement to limit the physical region illuminated (normally a cylindrical lens to convert a light beam to a line), asynchronizer to act as an external trigger for control of the camera and laser, the seeding particles and the fluid under investigation. A fiber optic cable or liquid light guide may connect the laser to the lens setup. PIV software is used to post-process the optical images.

5.2.1 Seeding

Seeding the flow with light reflecting particles is necessary in order to image the flow field. The particles should be small enough to follow the flow but large enough to reflect the required amount of light.

The particle distribution density is also important for the final analysis of a PIV process. In PIV a mid-density is needed for using cross correlation to measure the displacement.

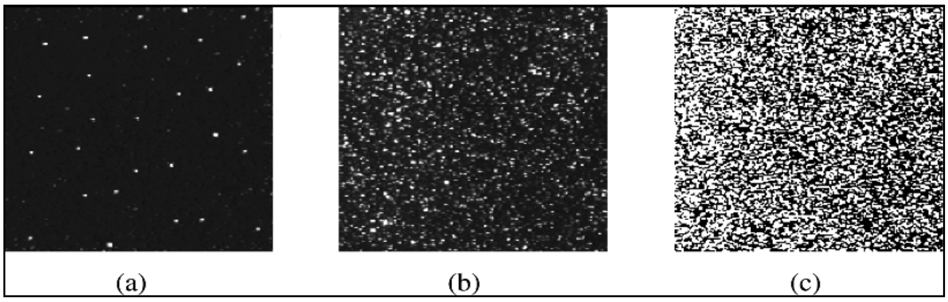

Figure 5.1 Different particle distribution densities (Raffel, Willert, Wereley, & Kompenhans, 2007)

Different particle densities is shown in Figure 5.1. The image (b) is suitable for PIV applications. A looser particle distribution like image (a) in Figure 5.1 will not support the velocity information from whole image. A denser particle distribution like image (c) in Figure 5.1 also cannot be used for cross correlation because the particle structure cannot be recognized in image pairs however this image can be used an elder method Particle Speckle Velocimetry which gives a general information about the flow structure.

5.2.2 Light Sources

Commonly a pulsed Nd:YAG laser (Neodymium Yttrium Aluminum Garnet) is used as the light source because of its high light intensity.

Nd:YAG lasers emit light with a wavelength of 1064 nm which is in the infrared range. For PIV-purposes light with this wavelength is not very useful since most cameras have their maximum sensitivity in the blue-green part of the spectrum. It is also disadvantageous not to be able to see the light sheet when positioning it in the measurement section. For these reasons the wavelength of the Nd:YAG laser is halved, using a device called a harmonic generator, so that it becomes 532 nm.

5.2.3 Cameras

PIV puts special demands on the camera that is going to be used, especially if the flow velocity is high, the imaged area is small. This circumstances requires the camera to be able to take two images within a short period of time in order for the same individual particles to appear in both images. Short exposure times can be achieved by having a high speed camera which continuously records images at a rate of several kHz. With a high speed camera the shortest inter image time possible today is around 10 μs and this is achieved by letting the first laser pulse come at the end of the exposure of the first image and the second pulse in the beginning of the exposure of the second image.

Cameras with progressive scan architecture can take two images with less than 1 μs delay. Directly after the first image has been recorded the charge of each pixel is transferred to its designated position in the interline shift register, a new image can now be recorded by the pixels. The second image is exposed until the first image has been read out from the interline shift register and is then transferred to the image buffer in the same way. The second image will due to this procedure be exposed for a longer time than the first and to avoid it becoming overexposed by ambient light a filter which only pass the laser wavelength can be fitted on the camera lens.

5.1.4 Synchronizer

The synchronizer acts as an external trigger for both the camera(s) and the laser. While analogue systems in the form of a photo sensor, rotating aperture and a light source have been used in the past, most systems in use today are digital. Controlled by a computer, the synchronizer can dictate the timing of each frame of the CCD camera's sequence in conjunction with the firing of the laser to within 1 ns precision. Thus the time between each pulse of the laser and the placement of the laser shot in reference to the camera's timing can be accurately controlled. Knowledge of this timing is critical as it is needed to determine the velocity of the fluid in the PIV analysis. Stand-alone electronic synchronizers, called digital delay generators, offer variable resolution timing from as low as 250 ps to as high as several ms. With up to eight channels of synchronized timing, they offer the means to control several flash lamps and Q-switches as well as provide for multiple camera exposures.

CHAPTER SIX
NUMERICAL STUDY AND VALIDATION

6.1 Introduction to Numerical Study

In this study, an outdoor unit of a residential split air conditioner has been investigated numerically. For this study, a Computer Aided Design (CAD) model of an outdoor unit has been taken from a factory which produces split air conditioners. The CAD model has been shown in Figure 6.1.

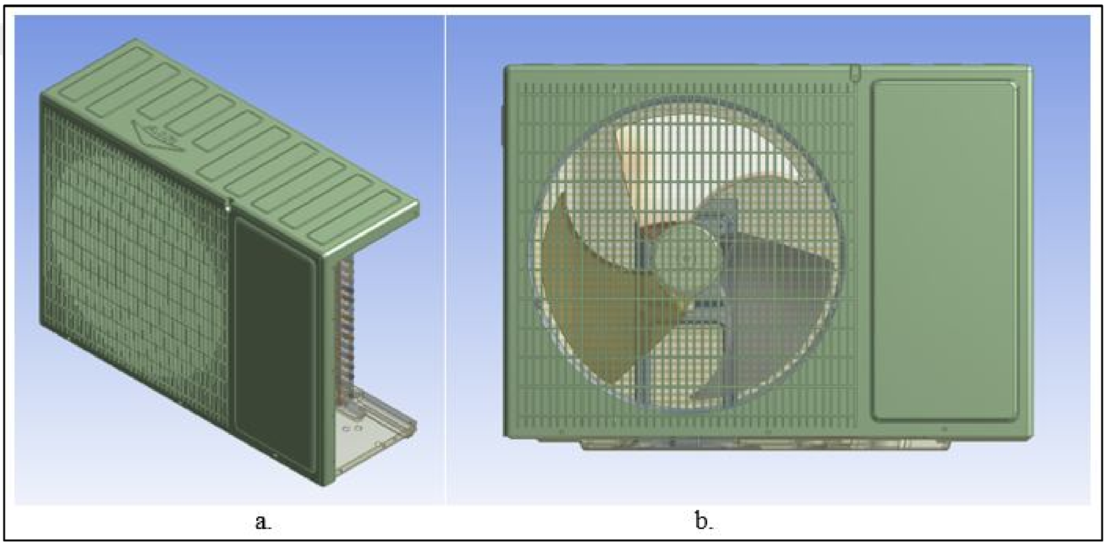

Figure 6.1 CAD model of outdoor unit: a) isometric view b) front view

CAD model includes four main parts: Axial fan, grille, heat exchanger and nozzle. The model also includes fan motor bracket because it is thought this part effects flow structure. The parts can be seen more detail in Figure 6.2.

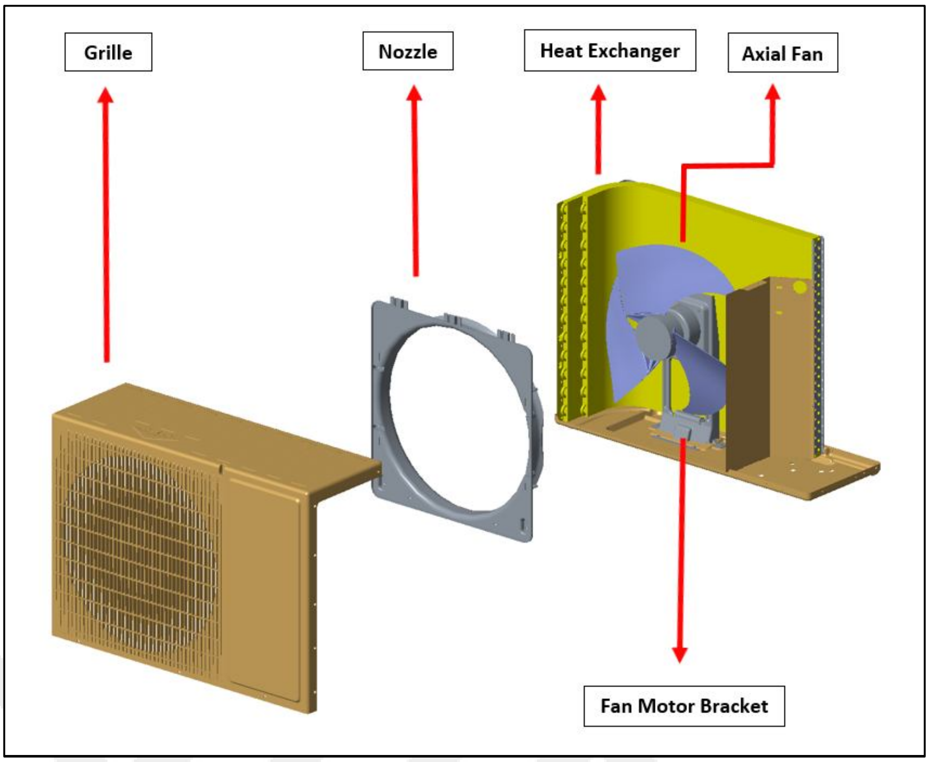

Figure 6.2 Parts of split air conditioner outdoor unit

6.2 Preparing CFD Model for Numerical Analysis

The flow structure was modelled three dimensionally for numerical study. To simplify CFD model, external walls of outdoor unit, solid parts haven't been modelled.

A stationary air volume has been created to define air, which is inside outdoor unit, for CFD model. Inside this air volume, a rotational air volume has also been generated for simulating axial fan's rotation.

For observing flow structure which is in front of outdoor unit, another air volume has been created. It can be seen in Figure 6.3.

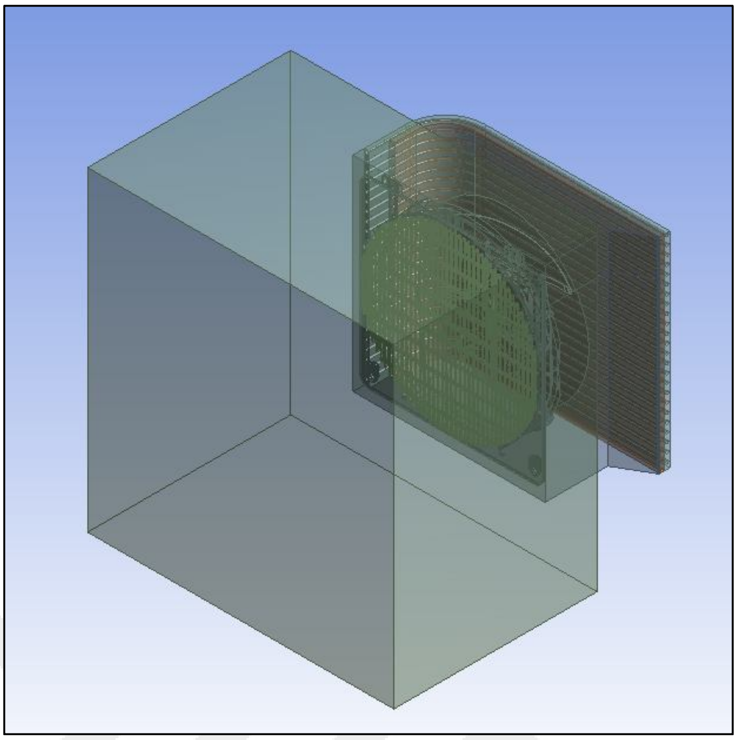

Figure 6.3 CFD model for numerical study

6.3 Meshing

Meshing is the most important process of CFD analyses for observing realistic results. It has a significant impact on rate of convergence, solution accuracy and CPU time required. For this study, different types of grids were generated. The mesh structure is shown in Figure 6.4. Tetrahedral mesh elements were used for most of parts, except heat exchanger. Tetrahedral elements are especially preferred when CFD model has complex geometries. Because these elements are more compatible with curvilinear faces. For meshing of heat exchanger, hexahedral meshes were created. If hexahedral elements were used instead of tetrahedral elements for some type of geometries, the number of mesh elements could much lower when compared with using of tetrahedral elements having same element sizing.

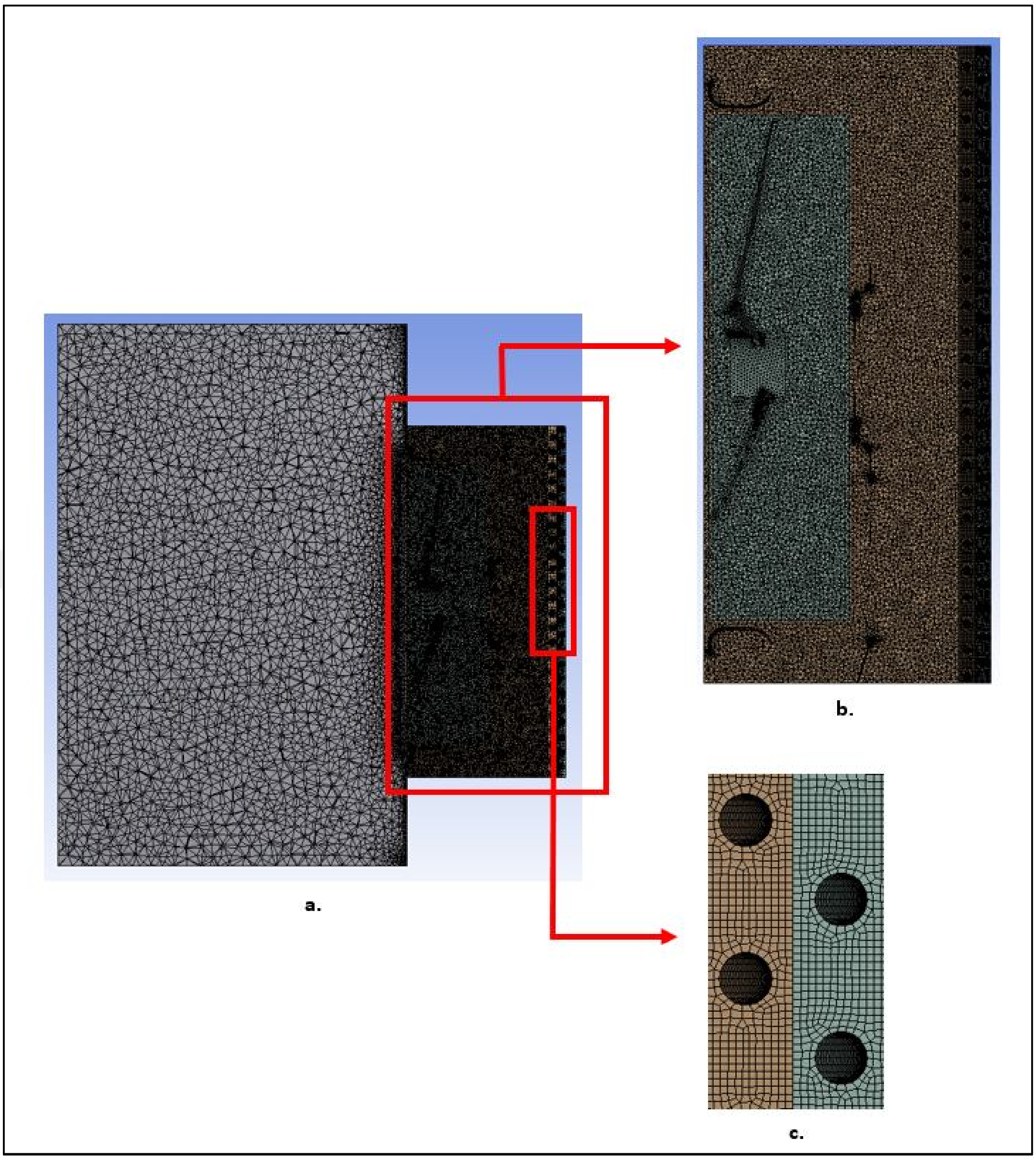

Figure 6.4 Mesh structure of numerical model: (a) mesh details of numerical model (b) mesh details of outdoor unit (c) mesh details of heat exchanger

In some region of numerical model, different element sizes were preferred to get more accurate results. Smaller elements were generated especially on fan blade surfaces, grille surfaces and outdoor unit's outlet. For deciding element size, mesh independency study was implemented. This study's result is shown in Figure 6.5. Mesh transition function is important because of creating smooth or abrupt transitions. It controls the rate at which elements grow. In this mesh independency study, ten cases were investigated with different number of elements by using both mesh transition functions. According to results, there is no big difference between fast and slow mesh transition. So, fast mesh transition function was preferred to reduce numerical calculation load and analysis time. Mesh independency study is shown in detail in Table 6.1.

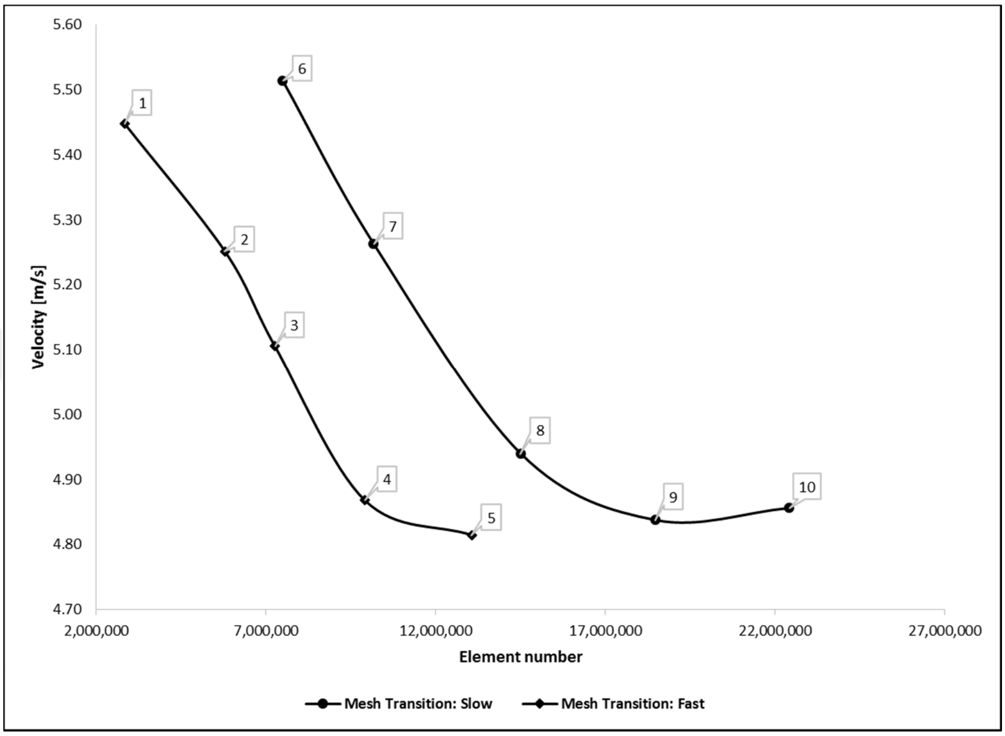

Figure 6.5 Average velocity values on outdoor unit's exit plane for different number of elements

Case 4 was chosen as final model. This model includes 8776631 tetrahedral elements, 1058165 hexahedral elements and 75416 wedge elements.

Table 6.1 Details of mesh independency study

Cases	Mesh Transition	Number of Elements	Average Velocity [m/s]
Case 1	Fast	2840742	5.45
Case 2	Fast	5790383	5.25
Case 3	Fast	7259786	5.11
Case 4	Fast	9910212	4.87
Case 5	Fast	13065899	4.81
Case 6	Slow	7492010	5.51
Case 7	Slow	10169328	5.26
Case 8	Slow	14505176	4.94
Case 9	Slow	18468599	4.84
Case 10	Slow	22416678	4.86

6.4 Boundary Conditions of CFD Model

Prepared model for analysis was transferred to CFD program for pre-processing. The parts were defined as fluid and porous domain. To reduce the computational load, solid domains weren't modelled.

In this numerical study, inner and outer ambient air domains were defined as stationary domain. Fan domain was introduced as a rotational domain with velocity of 980 RPM. Heat exchanger was described as a porous domain because it has too much thin fins. If it had been modelled as fluid domain, it had been too complex to resolve with grid. So, instead of including the geometric details, their effects were accounted for numerically.

k-ε turbulence model was chosen because of its wide capability. Heat transfer option wasn't activated because of examining only flow structure.

Opening boundary condition was defined for the surface where axial fan sucks air. This surface is the location where air enters the outdoor unit. After the domain, which represents the ambient air in front of outdoor unit, were defined as a fluid domain, the outer surfaces of this domain were defined by using opening boundary condition. Boundary conditions can be seen in Figure 6.6.

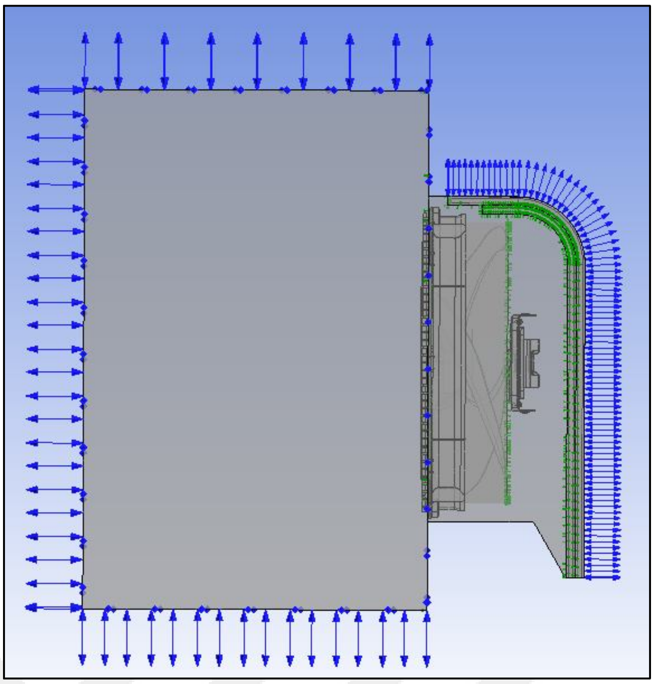

Figure 6.6 Boundary conditions of CFD model (top view)

The CFD model was solved by using transient type analysis during 2.5 seconds. The transient type analysis was performed instead of steady state analysis because average of time-resolved velocity contours required and this contours could be obtained from results which belonged to each timestep.

All numerical analyses have been done by utilizing Ansys CFX software.

6.5 Results of Numerical Solution

After the solution were completed, the convergence curves were obtained like in Figure 6.7 and Figure 6.8. According to the corvergence charts, it is seen that the air flow was reached to steady regime at the end of the numerical analysis.

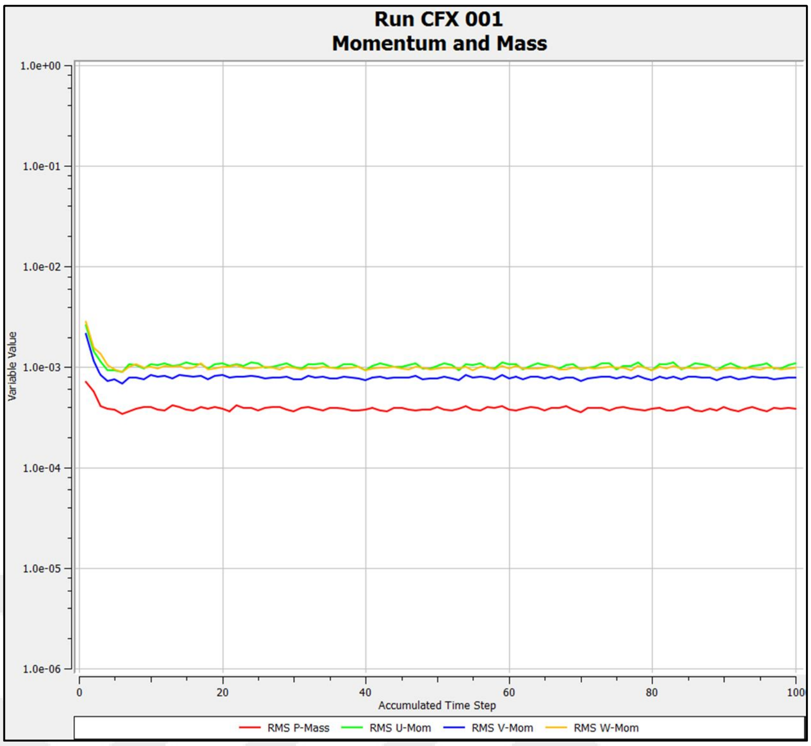

Figure 6.7 Momentum and mass residuals

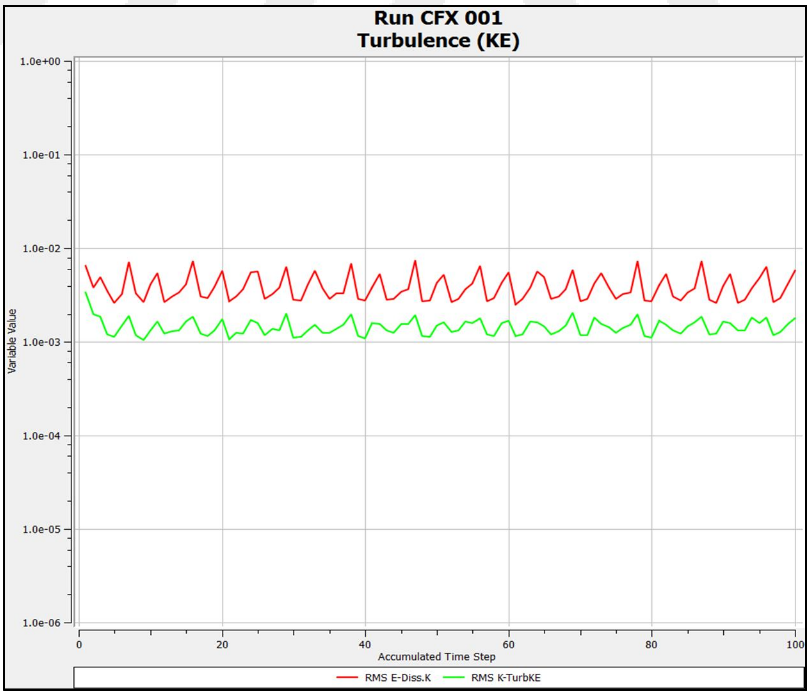

Figure 6.8 Turbulance residuals

Streamlines of flow structure were shown in Figure 6.9.

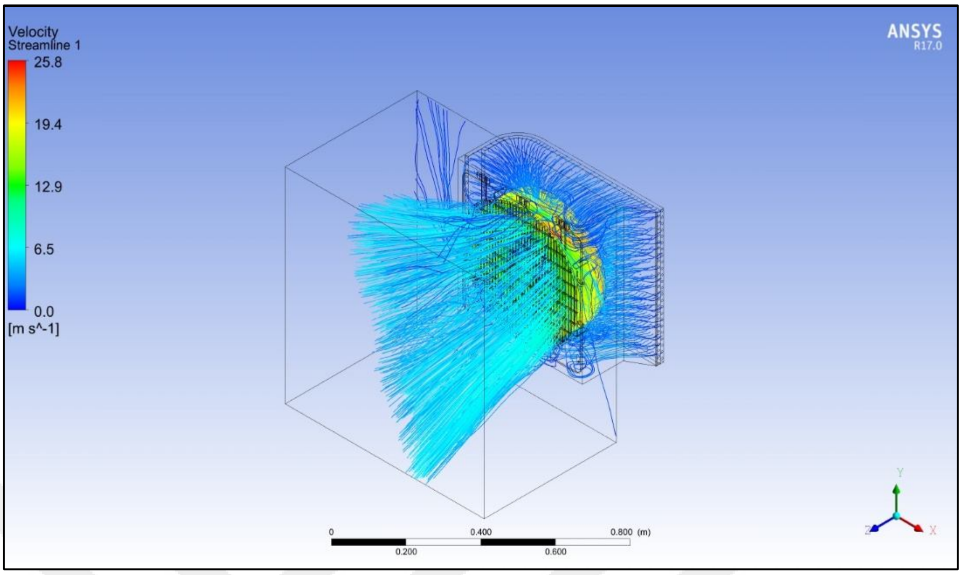

Figure 6.9 Streamlines of flow structure

As it is seen in Figure 6.9, the axial fan sucks the air from back side and then blows it to the environment. While the axial fan blows the air to the environment, the nozzle collects and directs the air and prevents the returning of air in the direction of axial fan.

6.6 Validation of Numerical Study

The results of numerical study were validated by experimental studies. Some experiments were performed and compared to the CFD analysis for obtaining more reliable results for validating flow field.

6.6.1 Velocity Verification

As an experimental method, PIV was used for validating exit velocity values and distribution in this study. PIV experimental setup consisted of laser, cameras, computer, synchronizer, fog generator. It is shown in Figure 6.10. Outdoor unit of split air conditioner was located along room axis. Thus, the effects on flow structure of walls, which is surrounded the room, was minimized.

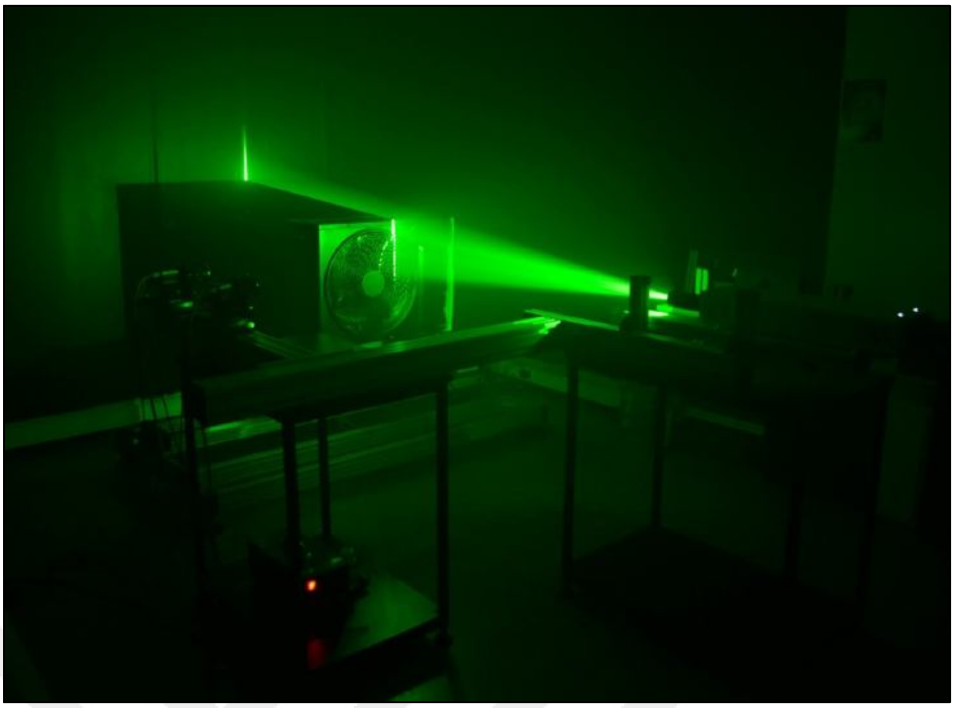

Figure 6.10 PIV experimental setup of outdoor unit

The relative positions of cameras, laser and measurement region are important for getting correct results. So, the cameras and laser were fixed to each other by using aluminum profiles. Thus, the relative positions of cameras and laser didn't change when these components moved for getting measurements from different planes. Two cameras were used in the experiment. One of them was placed perpendicularly to outdoor unit and the other one was placed angularly. The laser was positioned across outdoor unit for lightening the measurement region.

Seeding the flow with light reflecting particles is necessary in order to image the flow field. So, a fog generator was used to seed the flow. The successive images of particles were taken and the velocity vectors of measurement regions were obtained from these images by processing with a computer.

Outdoor unit's exit plane is shown in Figure 6.11. Average velocity of outdoor unit's exit plane, was calculated as 4.23 m/s according to numerical study result. The same velocity was acquired from PIV experiment as 3.74 m/s. Thus, the numerical model was validated with absolute velocity difference of 0.5 m/s.

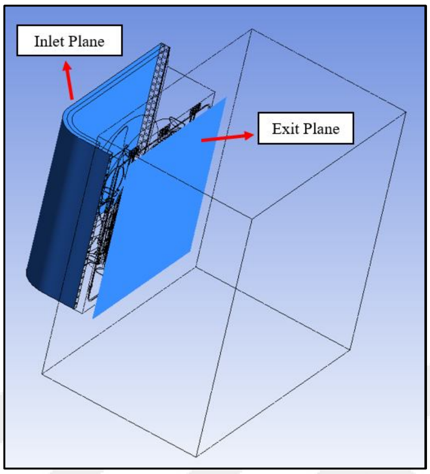

Figure 6.11 Investigation planes of outdoor unit

Velocity distribution and scale, which were acquired from numerical and experimental study, are shown in Figure 6.12.

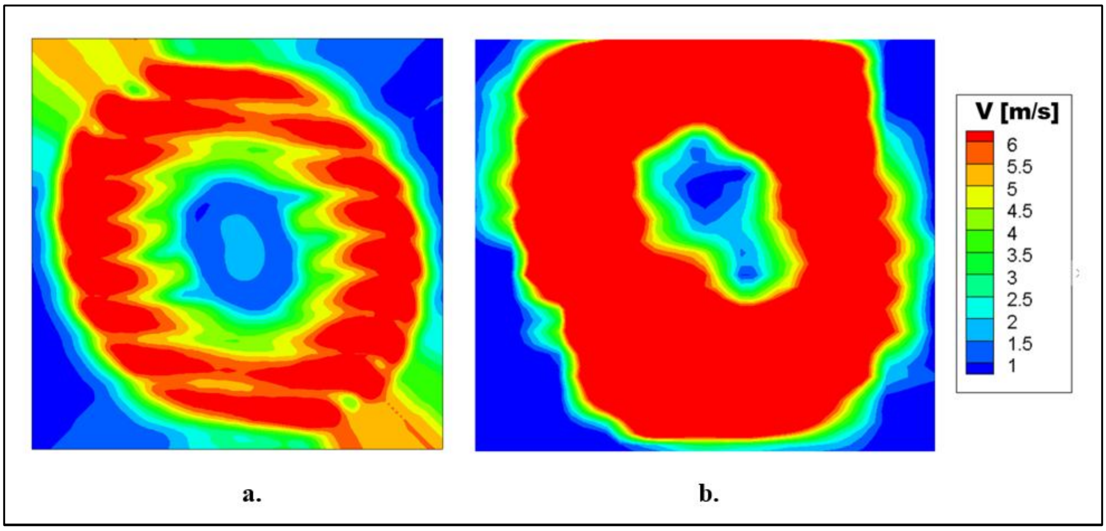

Figure 6.12 Velocity distribution and scale of outdoor unit's exit plane: a) numerical result b) experimental result

The numerical results for each timestep were imported and plotted velocity distribution contours like in Figure 6.12a. And the experimental results were obtained by taking thousands of images with a high resolution camera. And then the images were combined via Tecplot software, thus velocity contours were observed like in Figure 6.12b. When the two results were compared visually, it is seen that the largest velocity values occurred around the wing tips of axial fan. The velocity values reach to a range of 6 m/s around the wing tips. When it was approached towards to axial fan's center or it was gotten further away from axial fan's wing tips, velocity values decreased.

Like it is seen, the numerical and experimental results are consistent with each other.

6.6.2 Mass Flow Rate Verification

Another experiment for validating CFD results is to measure air mass flow rate of outdoor unit's exit plane. The experimental setup is shown in Figure 6.13.

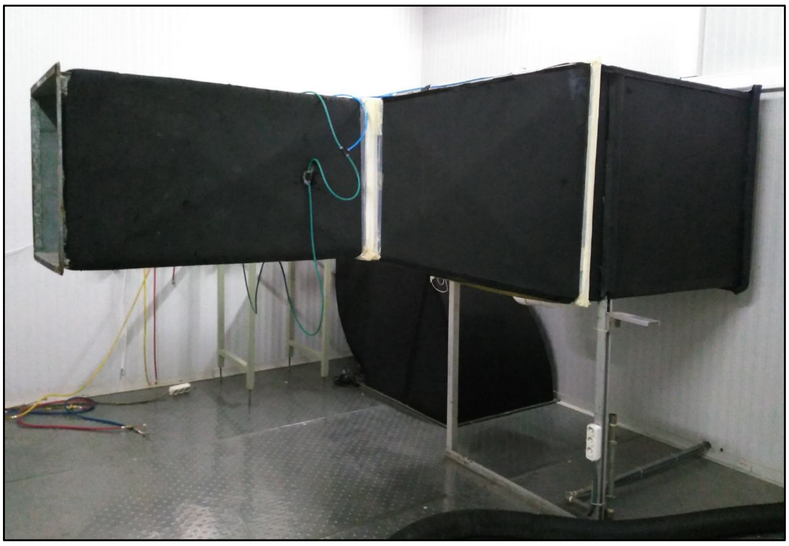

Figure 6.13 Experimental setup for measuring mass flow rate

The measurement channel was located in a way that it covered outdoor unit's front boundary. Then outdoor unit's axial fan was driven by a motor externally. The air mass flow rate which were blowed by axial fan was measured through a flowmeter at the exit of outdoor unit.

As a result of experiment, the average mass flow rate of air on outdoor unit's exit plane was obtained as 2090 m^3/h. On the other hand, it was acquired as 2081.12 m^3/h from numerical study. Second validation of numerical model was performed with the error 0.42%.

CHAPTER SEVEN
PARAMETRIC STUDY

The design parameters were investigated after validation of CFD model. The parameters, which would have major effects on flow structure, were decided. The geometrical characteristics of these parameters are shown in Figure 7.1.

The geometrical characteristics were investigated in a non-dimensional form. This non-dimensional form was defined as $D_1 / D = 1.06$, $H_1 / H = 1.82$, $H_2 / H = 0.48$, $H_3 / H = 0.41$. These are non-dimensional input parameters. Here, D (mm) is the diameter of axial fan, D_1 (mm) is the diameter of nozzle, H (mm) is the depth of axial fan, H_1 (mm) expresses the positon of heat exchanger, H_2 (mm) is the depth of nozzle and H_3 (mm) expresses the positon of axial fan.

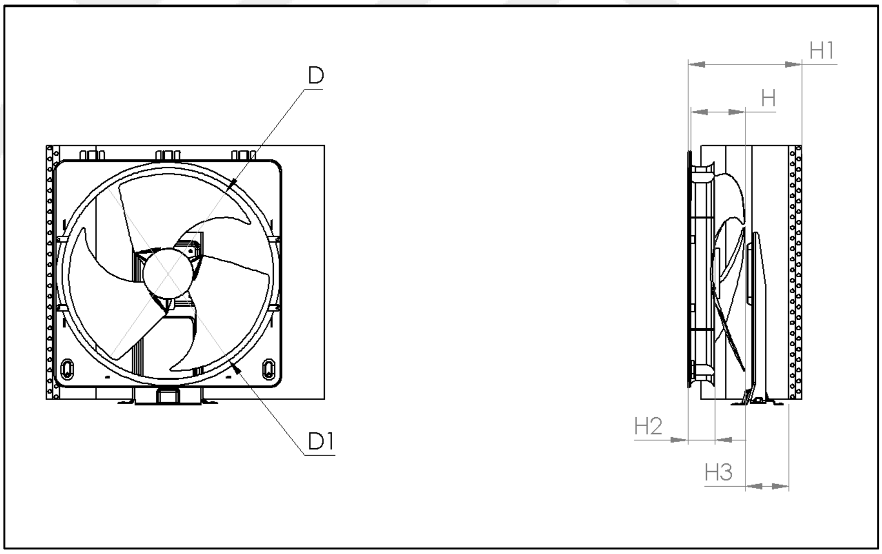

Figure 7.1 Geometrical characteristics of outdoor unit: (a) front view (b) right side view

The output parameters were expressed in another non-dimensional form. According to the literature, the pressure and flow coefficients (Eck, 1973) are used to determine the performances of different types of fan. So, pressure coefficient (Ψ) and flow coefficient (Φ) were used for evaluating the parametric investigation results in this study. The pressure coefficient is

$$\Psi = \Delta P / (\rho / 2)\, U_{tip}^2 \tag{7.1}$$

where ΔP (Pa) is average total pressure rise of air, ρ (kg / m^3) is density of air, U_{tip} (m/s) is tip speed of axial fan. ΔP is the total pressure difference between average total pressure of inlet plane and average total pressure of exit plane. These planes were shown in Figure 6.11 for this study.

The flow coefficient is

$$\Phi = Q / [\, (\pi D^2 / 4)\, U_{tip} \,] \tag{7.2}$$

where Q (m^3 / s) is average mass flow rate of air on exit plane and $\pi D^2 / 4$ (m^2) is cross sectional area of axial fan.

7.1 Effects of Nozzle Depth

The nozzle is an important component because it collects and directs the air flow which is blown by axial fan. So, the geometrical properties of the nozzle affect the flow structure significantly.

Firstly, nozzle depth was investigated as a design parameter. Three different geometrical characteristics were investigated and these are shown in Table 7.1.

Table 7.1 The design parameters of nozzle depth

Non–dimensional form of nozzle depth's geometrical characteristic	**Non-dimensional parameters**
H_2 / H	0.57
	0.66
	0.75

CFD analyses were repeated for three different geometrical characteristics. The results are shown in Figure 7.2. When nozzle depth increases, pressure and flow coefficients decrease. So, current nozzle depth has the best value among investigated parameters.

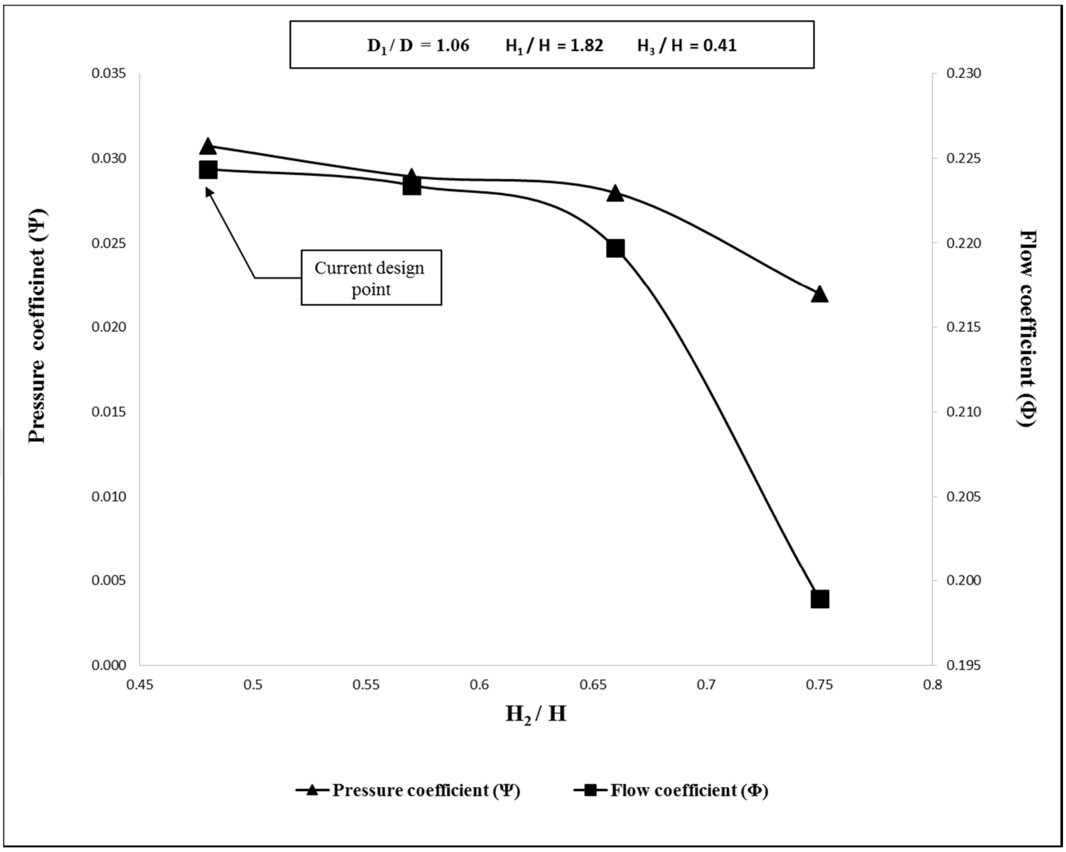

Figure 7.2 Effects of nozzle depth

7.2 Effects of Nozzle Diameter

Another important geometrical characteristic is nozzle diameter. According to the limits of mechanical construction, nozzle diameter was investigated for four different parameters. These parameters are shown in Table 7.2.

Table 7.2 The design parameters of nozzle diameter

Non–dimensional form of nozzle diameter's geometrical characteristic	Non-dimensional parameters
D_1 / D	1.04
	1.05
	1.08
	1.09

After numerical analyses were performed, the results were obtained like in Figure 7.3. According to results, performance coefficients increased with descending nozzle diameter. The coefficients decreased with ascending nozzle diameter. In this condition, the pressure and flow coefficients were increased by 6.94 % and 2.91 % respectively according to current design.

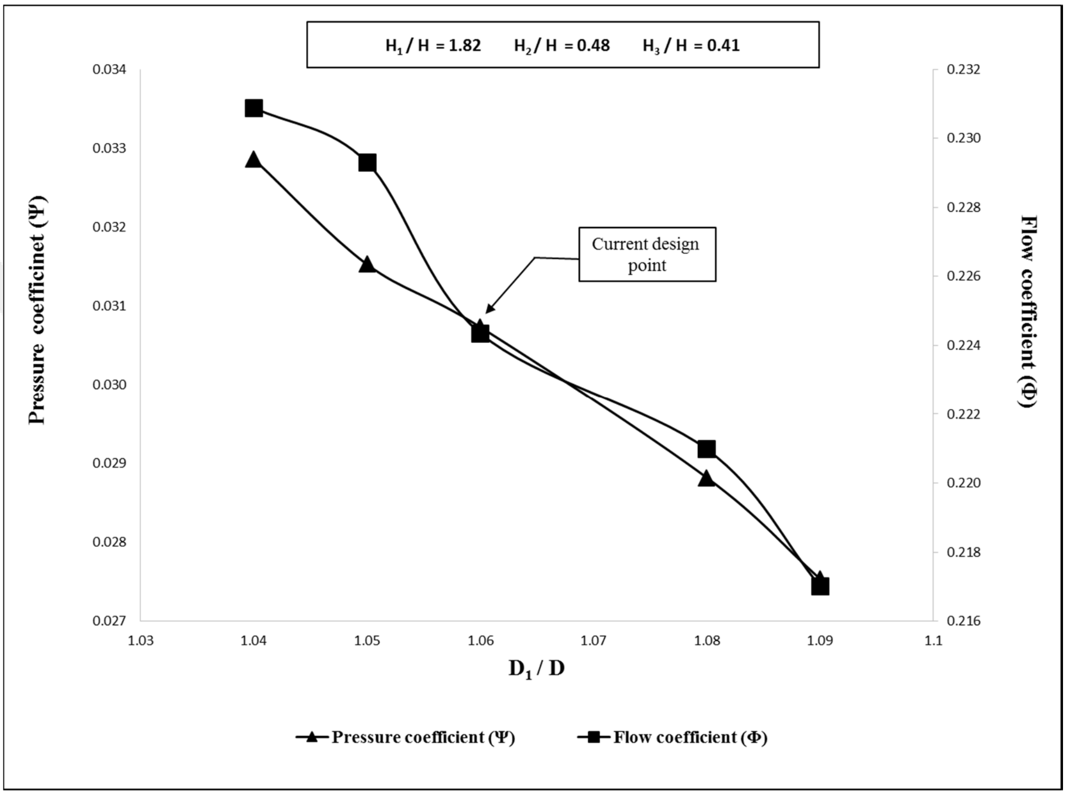

Figure 7.3 Effects of nozzle diameter

7.3 Effects of Fan Position

Axial fan is the most important part in an outdoor unit of a split air conditioner. It sucks the hot air which is heated by heat exchanger and then blows it to the environment. It has significant effects on outdoor air unit’s performance. So, fan position was decided to investigate.

There is no place to translate for bringing the axial fan closer to the nozzle because of mechanical construction limits. So, three different fan positions were chosen. The parameters for this geometrical characteristic are shown in Table 7.3.

Table 7.3 The design parameters of fan position

Non–dimensional form of fan position's geometrical characteristic	Non-dimensional parameters
H_3 / H	0.11
	0.21
	0.31

The numerical results which were obtained by analyses are shown in Figure 7.4. When the axial fan was moved away from the nozzle, the pressure and flow coefficients decreased. So, current fan position is the best position among investigated parameters.

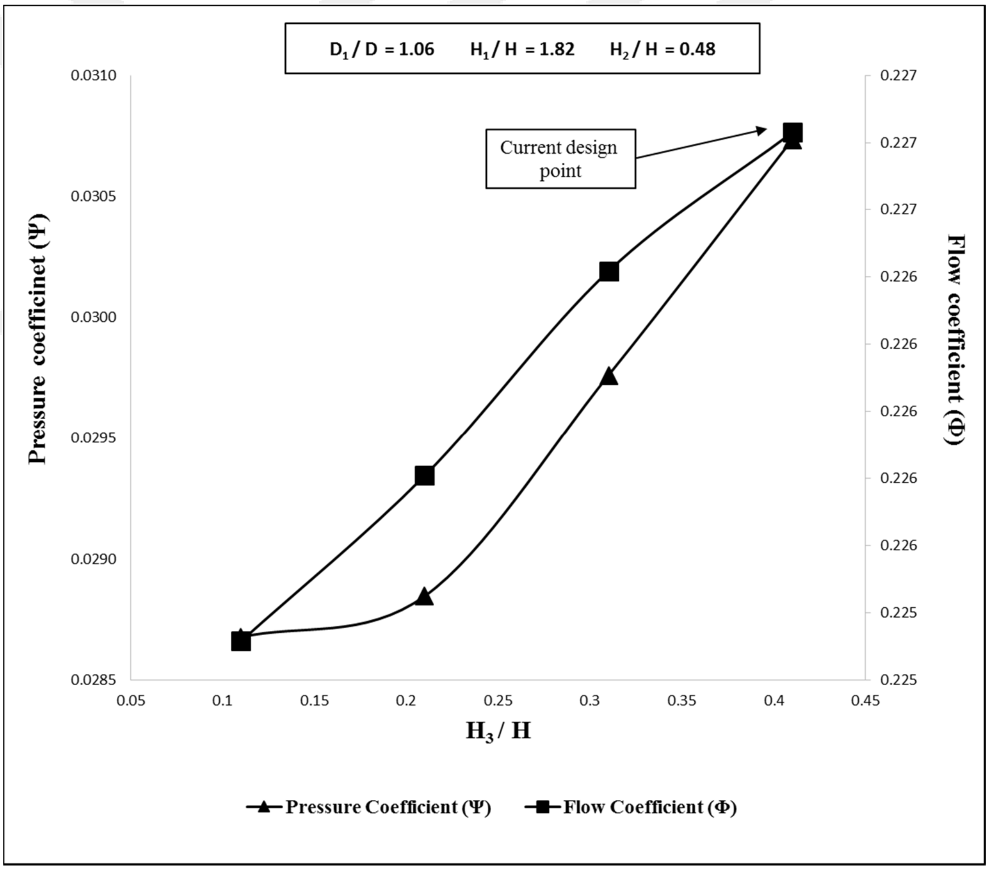

Figure 7.4 Effects of fan position

7.4 Effects of Heat Exchanger Position

Heat exchanger is another component which affects flow structure and pressure change. So heat exchanger position is a significant parameter. It doesn't only influence flow structure, but also the size of outdoor unit. The numerical analyses were performed for five different heat exchanger positions. The parameters are like in Table 7.4.

Table 7.4 The design parameters of heat exchanger position

Non–dimensional form of heat exchanger's geometrical characteristic	**Non-dimensional parameters**
	1.62
	1.72
H_1 / H	1.92
	2.02
	2.12

The results are shown in Figure 7.5. When heat exchanger was moved away from axial fan, the pressure and flow coefficients ascended. On the contrary, if heat exchanger was got closer to the fan, the coefficients descended. It is seen from the results that the optimum heat exchanger position was acquired when the geometrical characteristic H_1 / H was 2.12. The pressure and flow coefficients were increased by 2.00 % and 2.19 % respectively in this case.

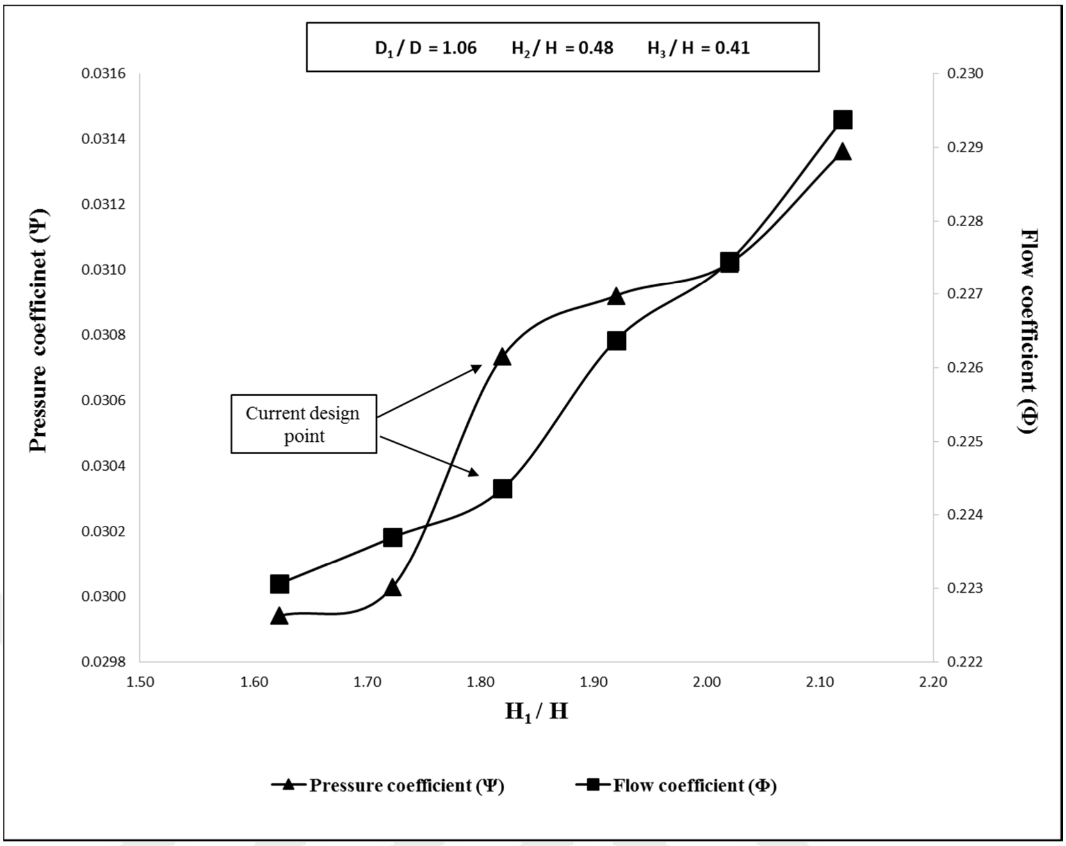

Figure 7.5 Effects of heat exchanger position

7.5 Effects of Nozzle Diameter, Fan Position and Heat Exchanger Position

The types of parameters were investigated separately, but the interactions of these parameters with each other have to be investigated for determining optimum pressure and flow coefficients among investigated parameters. The design parameters, which were more effective for performance coefficients, were decided to be changed simultaneously instead of alternating all parameters at the same time. An analysis tree was created for expressing which numerical analyses should have been performed to get optimum coefficients. This analysis tree is similar to the test tree which was used by Lazzarotto et al. It is shown in Figure 7.6.

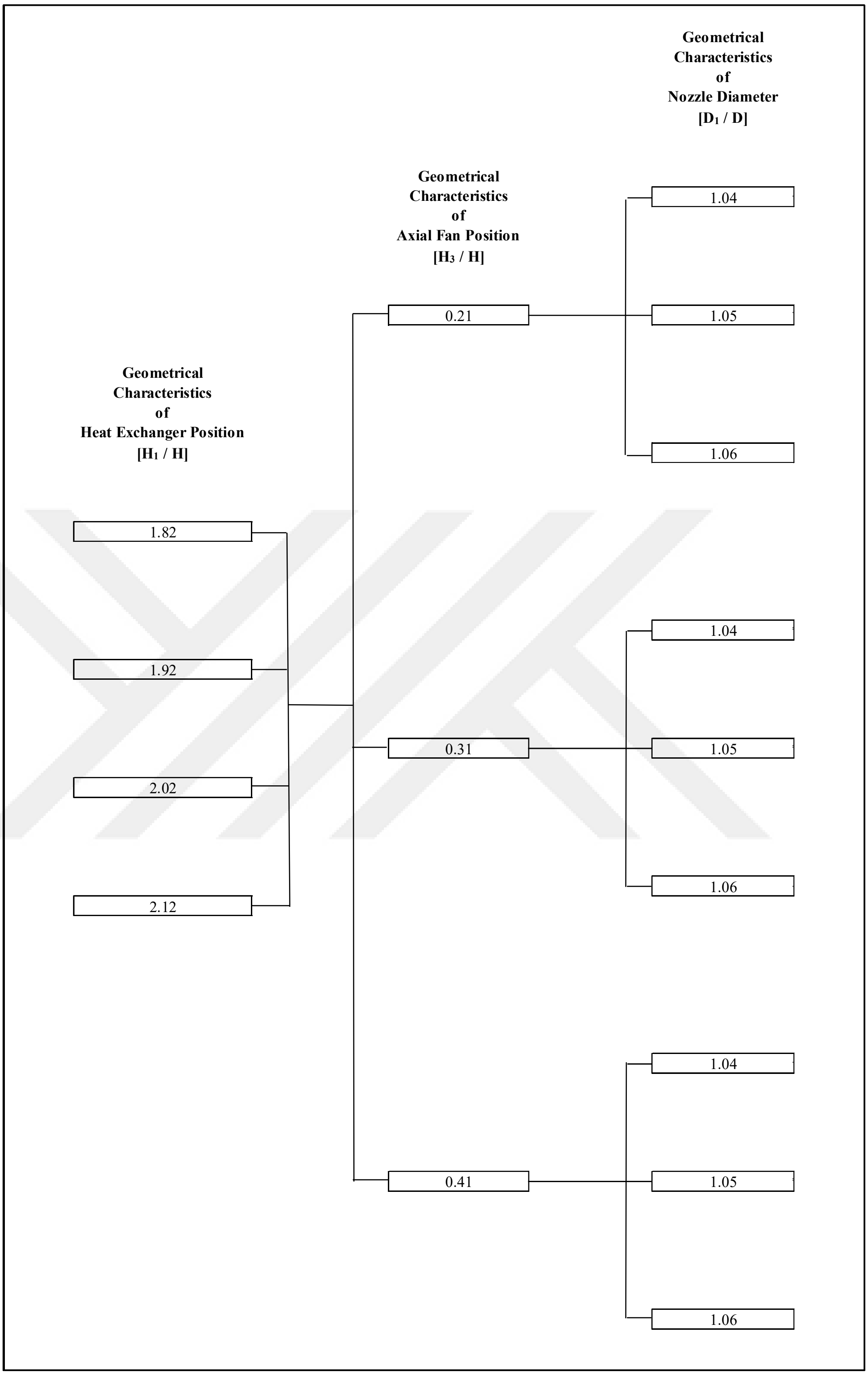

Figure 7.6 Numerical analysis tree

According to the analysis tree, numerical analyses were performed for 36 different design points. The first results are shown in Figure 7.7.

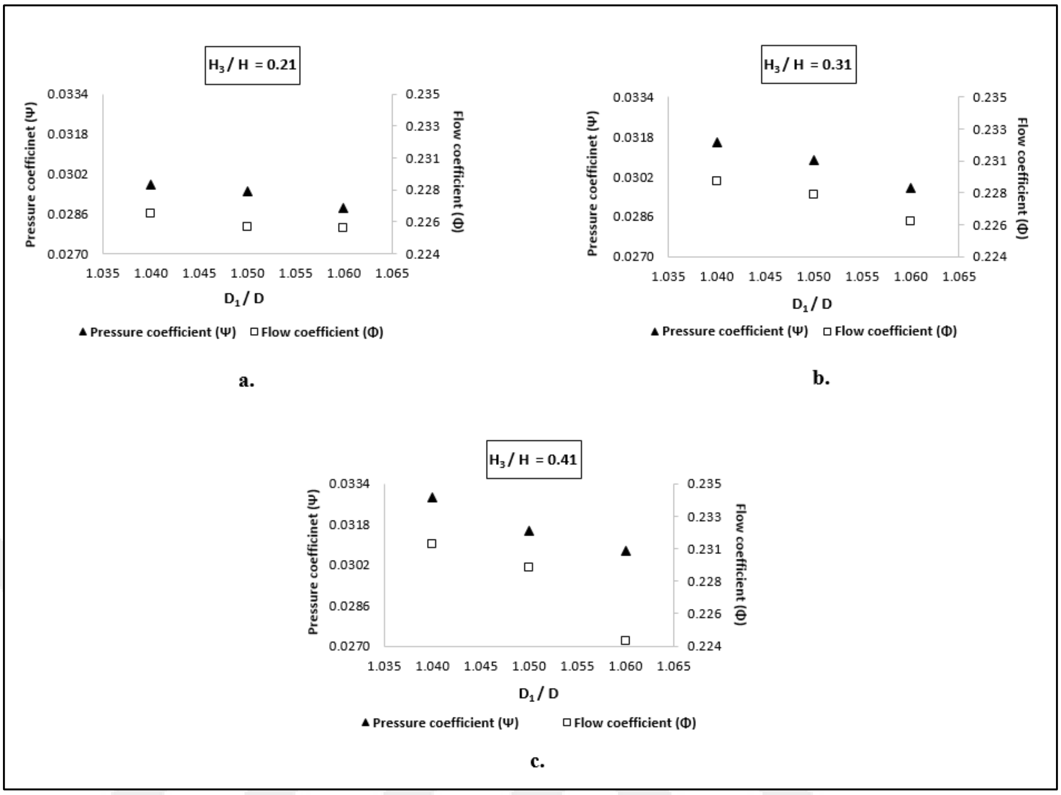

Figure 7.7 Numerical results for H_1 / H = 1.82

By observing the results obtained from parametric study in Figure 7.7a, it is apparent that there are no significant change on pressure and flow coefficients. Although the geometrical characteristic of D_1 / D increases, the values of performance coefficients don't change significantly. However, the pressure and flow coefficients have increasingly higher values when fan position's geometrical characteristic of H_3 / H increases like in Figure 7.7b and Figure 7.7c. In addition, nozzle diameter's geometrical characteristic of D_1 / D has more significant effects on performance coefficients for H_3 / H = 0.31 and H_3 / H = 0.41 when compared to H_3 / H = 0.21. When H_3 / H increases, D_1 / D has larger effects on pressure and flow coefficients and also the performance coefficients have higher values.

The rest of the parametric results are shown in Figure 7.8, Figure 7.9 and Figure 7.10.

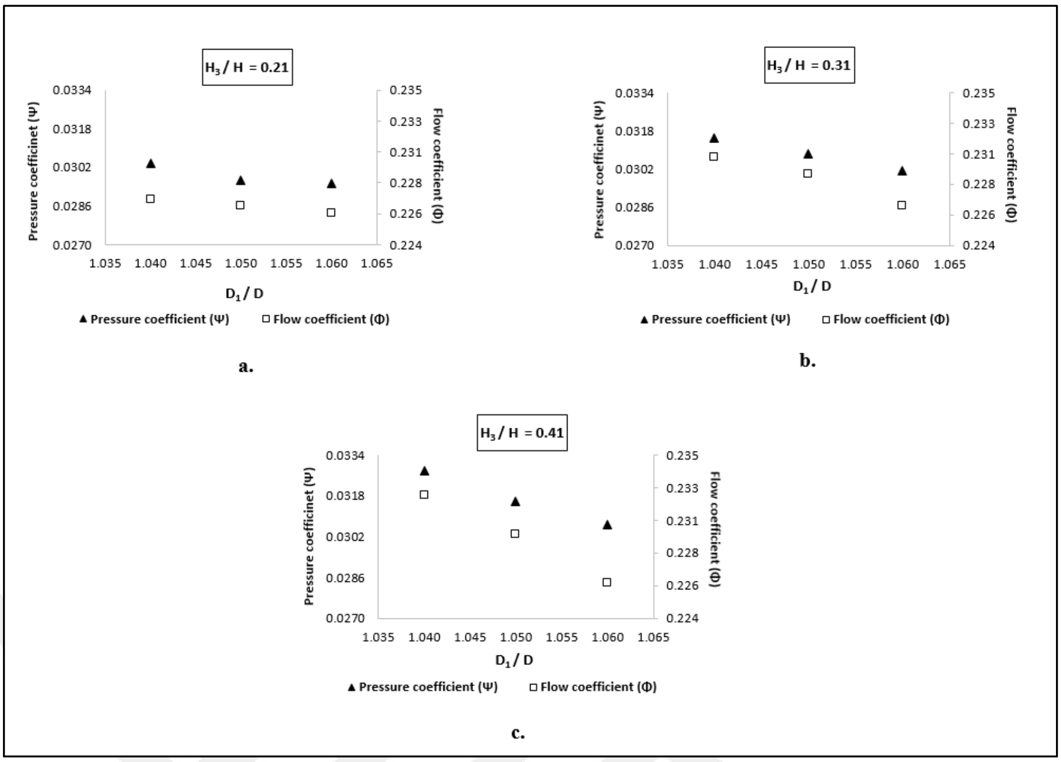

Figure 7.8 Numerical results for H_1 / H = 1.92

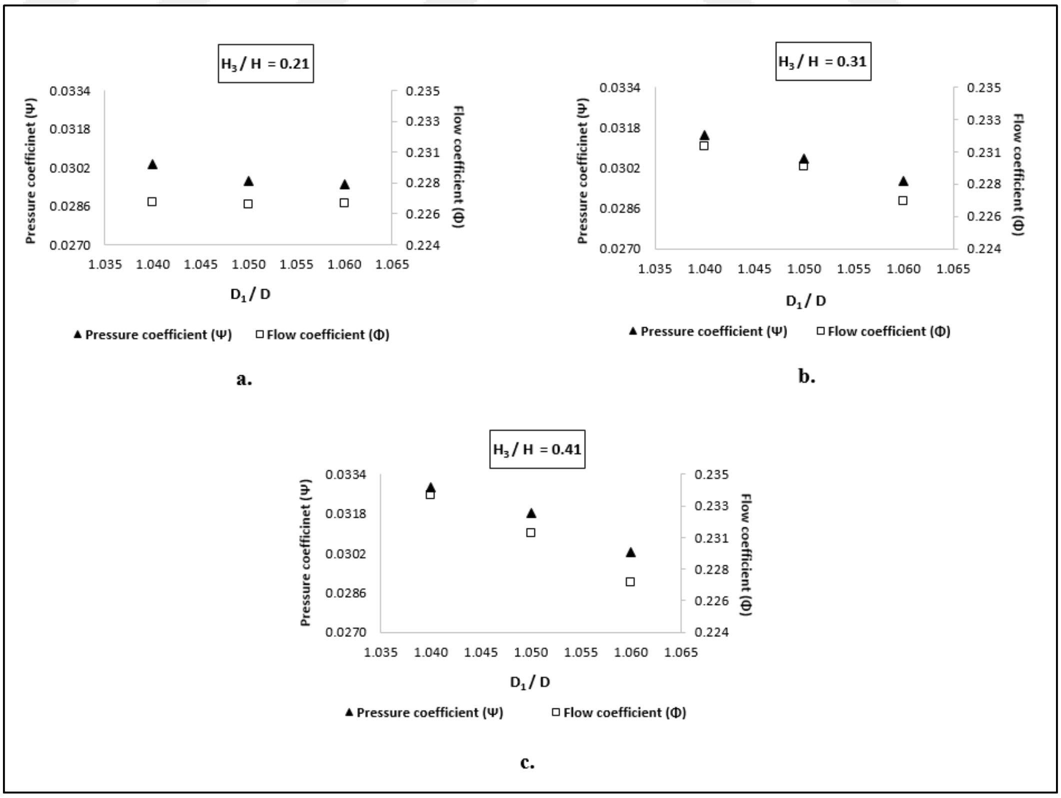

Figure 7.9 Numerical results for H_1 / H = 2.02

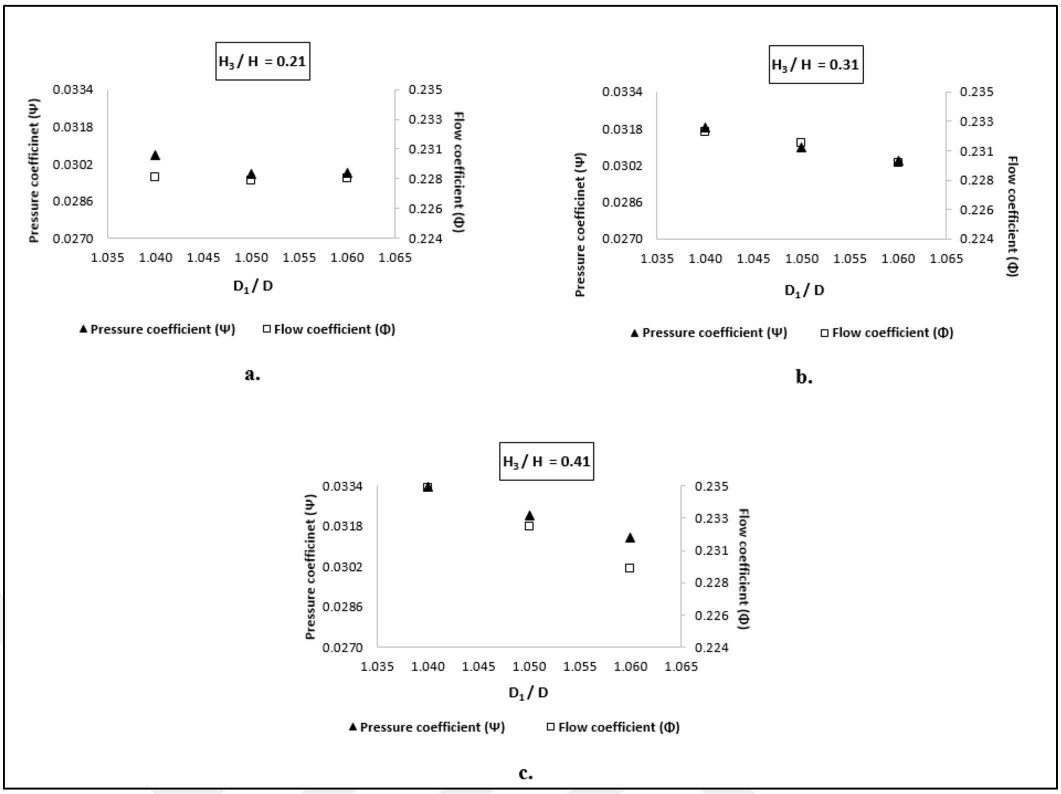

Figure 7.10 Numerical results for H_1 / H = 2.12

When the results in Figures 7.8a – 7.8c, Figures 7.9a – 7.9c and Figures 7.10a – 7.10c are examined, they have similar relationships like the results in Figures 7.7a – 7.7c.

If the results are compared to each other in Figures 7.7a – 7.10a, the performance coefficients have higher values progressively, but the values of enhancement are not significant. The results in Figures 7.7b – 7.10b and Figures 7.7c – 7.10c have similar conditions. It is seen that the geometrical characteristic of heat exchanger H_1 / H doesn't have noticeable effects on performance coefficients.

According to all results in this parametric study, the optimum performance coefficients were obtained for the design point where D_1 / D = 1.04, H_3 / H = 0.41 and H_1 / H = 2.12 were. The optimum design point is in Figure 7.10c. and it has 7.82 % higher pressure coefficient and 4.48 % higher flow coefficient when compared to current model.

CHAPTER EIGHT
CONCLUSIONS

In this study, an outdoor unit of a split air conditioner were investigated numerically. The outdoor unit was modelled three dimensionally in a software. Then, this numerical model was solved under transient state condition by using the method of computational fluid dynamics (CFD). The outdoor unit's flow structure was also investigated by using particle image velocimetry (PIV) method. This experimental method was used for validating numerical model. For another verification, the measurement of air mass flow rate blowing by axial fan was performed experimentally.

After the validation, optimum geometrical values of nozzle diameter, nozzle depth, fan position and heat exchanger position were investigated by performing parametric study. The geometrical parameters were examined both separately and simultaneously for improving performance coefficients.

In literature, there isn't any study whose subject is about investigation of split air conditioner's outdoor unit by CFD. As a contribution to the literature, an outdoor unit would be solved numerically, the flow structure of the outdoor unit could be investigated for different geometrical parameters and the outdoor unit's flow performance would be improved by this method, which was explained in this thesis. In addition, it is possible to reduce prototype costs and time by implementing this method. The effects such as reducing nozzle diameter or changing fan position can be performed to examine possible results by implementing similar analyses numerically.

REFERENCES

Air conditioning. (n.d.). Retrieved February 3, 2016, from https://en.wikipedia. org/wiki/ Air_conditioning.

Air conditioners. (n.d.). Retrieved February 3, 2016, from http://www.whirlpoolindia. com/blog/cooling/air-conditioner/the-truthaboutthe-hot-wind-expelled-fromaircon ditioners#pretty.

Avara, A., & Daneshgar, E. (2008). Optimum placement of condensing units of split-type air-conditioners by numerical simulation. *Energy and Buildings, 40*, 1268–1272.

Blazek, J. (2001). *Computational fluid dynamics: Principles and applications*. (1st ed.). Netherlands: Elsevier Science Ltd.

Chow, T. T., Lin, Z., & Liu, J. P. (2002). Effect of condensing unit layout at building re-entrant on split-type air-conditioner performance. *Energy and Buildings, 34*, 237–244.

Chow, T. T., Lin, Z., & Wang, Q. W. (2000). Effect of building re-entrant shape on performance of air-cooled condensing units. *Energy and Buildings, 32*, 143–152.

Cooling the planet: Opportunities for deployment of superefficient room air conditioners (2013). Retrieved February 3, 2016, from https://superefficient.org.

Çengel, Y. A., & Boles, M. A. (2006). *Thermodynamics an engineering approach* (5th ed.). New York: McGraw-Hill.

Eck, B. (1973). *Fans* (1st ed.). U.S.A: Pergamon Press.

Energy efficiency reference guide: Fans and blowers. (n.d.). Retrieved February 3, 2016, from https://www.bchydro.com/content/dam/hydro/medialib/internet/documents/psbusiness/pdf/fans_ blowers_ guide.pdf.

Foss, J. F., Morris, S. C., & Neal, D. R. (n.d.). *Tech Brief: Axial fan research for automotive and building ventilation applications*. Retrieved May 22, 2016, from http://www.egr.msu.edu/tsfl/Publications/ASME_FED_Newsletter_2001_tech_brief_only.pdf.

Falahat, A. (2011). Numerical and experimental optimization of flow coefficient in tubeaxial fan. *International Journal of Multidisciplinary Sciences and Engineering, 2* (5), 24-29.

Hu, J., & Ding, G. (2006). Effect of the air outlet louver on the noise generated by the outdoor set of a split-unit air conditioner. *Applied Thermal Engineering, 26*, 1737–1745.

Hu, J., & Ding, G. (2006). Effect of deflecting ring on noise generated by outdoor set of a split-unit air conditioner. *Internal Journal of Refrigeration, 29*, 505–513.

Hu, S. S., & Huang, B. J. (2005). Study of a high efficiency residential split water-cooled air conditioner. *Applied Thermal Engineering, 25*, 1599–1613.

Lazzarotto, L., Lazzaretto, A. & Martegani, A. D. (2001). On cross-flow fan similarity: Effects of casing shape. *Journal of Fluid Engineering, 123*, 523–531.

Moran, M. J., Shapiro, H. N., Boettner, D. D., & Bailey, M. B. (2014). *Fundamentals of engineering thermodynamics* (8th ed.). USA: Wiley.

Özer, Ö. (2011). *Experimental investigation of velocity and temperature distribution inside a split air conditioner indoor unit.* M.Sc. Thesis, Dokuz Eylül University, İzmir.

Particle image velocimetry. (n.d.). Retrieved April 6, 2016, from https://en.wikipedia.org/wiki/Particle_image_velocimetry.

Raffel, M., Willert C., Wereley, S., & Kompenhans, J., (2007). *Particle image velocimetry a practical guide* (2nd ed.). New York: Springer.

Zhao, X., Sun, J., Wang, C., & Zhang Z. (2014). Experimental and numerical study of electronic module-cooling heat sinks used in a variable frequency air-conditioner outdoor unit. *International Journal of Refrigeration, 36*, 10–21.

Zhao, X., Sun, J., & Zhang Z. (2013). Prediction and measurement of axial flow fan aerodynamic and aeroacoustic performance in a split-type air-conditioner outdoor unit. *International Journal of Refrigeration, 36*, 1098–1108.